Physical Environment

Ecosystem Indicators and Trends Used by FOCI - 2006

Edited by S. Allen Macklin, NOAA/PMEL
Contact: S.Allen.Macklin@noaa.gov

Last updated: November 2006

FOCI's scientists employ a number of climate, weather, and ocean indices and trends to help describe and ascribe the status of the ecosystem to various patterns or regimes. This document presents some of these with respect to current (2004) conditions. This section begins with an overview of North Pacific climate for 2004, including an examination of trends and tendencies in multidecadal and decadal climate regimes. Following this section are sections dealing explicitly with the western Gulf of Alaska and eastern Bering Sea. Within these are continuations of discussions begun in 2003 on eddy kinetic energy in the Gulf of Alaska and modeled drift trajectories for the Bering Sea.

Pacific Climate Overview

S. Rodionov, J. Overland, and N. Bond (NOAA PMEL)
Contact: Sergei.Rodionov@noaa.gov

Last updated: November 2006

Summary. *Atmospheric circulation over the North Pacific during 2006 was characterized by a high degree of variability. A strong Aleutian low, which dominated in December 2005, substantially weakened and split into two centers in January 2006. The anomalous high pressure center that formed over the central North Pacific is consistent with the weak La Niña that was present in the tropical Pacific. The anomalous atmospheric circulation was accompanied by a southward expansion of negative sea surface temperature anomalies in the Gulf of Alaska and a relatively warm water pool in the North Pacific near the dateline that persisted through spring and summer of 2006. There are conflicting signals regarding the evolution of North Pacific SST anomalies into 2007. Coupled GCM forecasts from the Climate Prediction Center suggest persistence of the current SST anomaly pattern into early 2007. On the other hand, a weak to moderate El Nino is forming in the fall of 2006, which often is associated with a stronger than normal Aleutian low, which itself usually acts to cool the central North Pacific and bring about a narrow strip of warmer than normal water along the North American coast. A great deal of ambiguity still exists regarding a possible climate regime shift in the late 1990s. Some indices, such as the winter PDO index from N. Mantua and Pacific/North American (PNA) index, lack substantial and systematic changes in their states. An alternative version of the winter PDO index from National Climate Data Center and summer PDO index, however, feature statistically significant shifts to negative values in 1998/99. That time also corresponds to a statistically significant shift in the El Niño/ Southern Oscillation.*

1. El Niño – Southern Oscillation (ENSO)

During September 2005- January 2006, below-average SSTs developed throughout most of the central and eastern equatorial Pacific. In February 2006 positive SST anomalies developed in the extreme eastern equatorial Pacific, similar to what occurred in 1999, 2000 and 2001 (La Niña years). Based on the Oceanic Niño Index (ONI), which has become the de-facto standard used by NOAA to identify ENSO events, these conditions in the equatorial Pacific qualified as a weak La Niña episode (Figure 11).

Recently, SST anomalies have increased in the west-central and extreme eastern equatorial Pacific to qualify for a weak El Niño event. Statistical and coupled model forecasts produced by the Climate Prediction Center suggest that there is a potential for this event to strengthen into a moderate event by winter. However, the spread of these forecasts indicates considerable uncertainty in the outlook for late 2006 and early 2007.

2. Arctic Sea-Ice

The warming trend in the Arctic is illustrated in Figure 12, which shows the Northern Hemisphere sea ice extent in March, as measured from passive microwave instruments onboard NOAA satellites. March is the month when Arctic sea ice reaches its maximum extent. The overall downward trend in the sea ice extent has accelerated in the past four years. In 2006 it was 14.5 million square kilometers, the lowest value for any March on record (Figure 12). This is 1.2 million square kilometers below the long-term (1979-2000) mean. The implications of this trend for the North Pacific are likely to include a tendency for a shorter season during which intense cold-air outbreaks of arctic origin can occur.

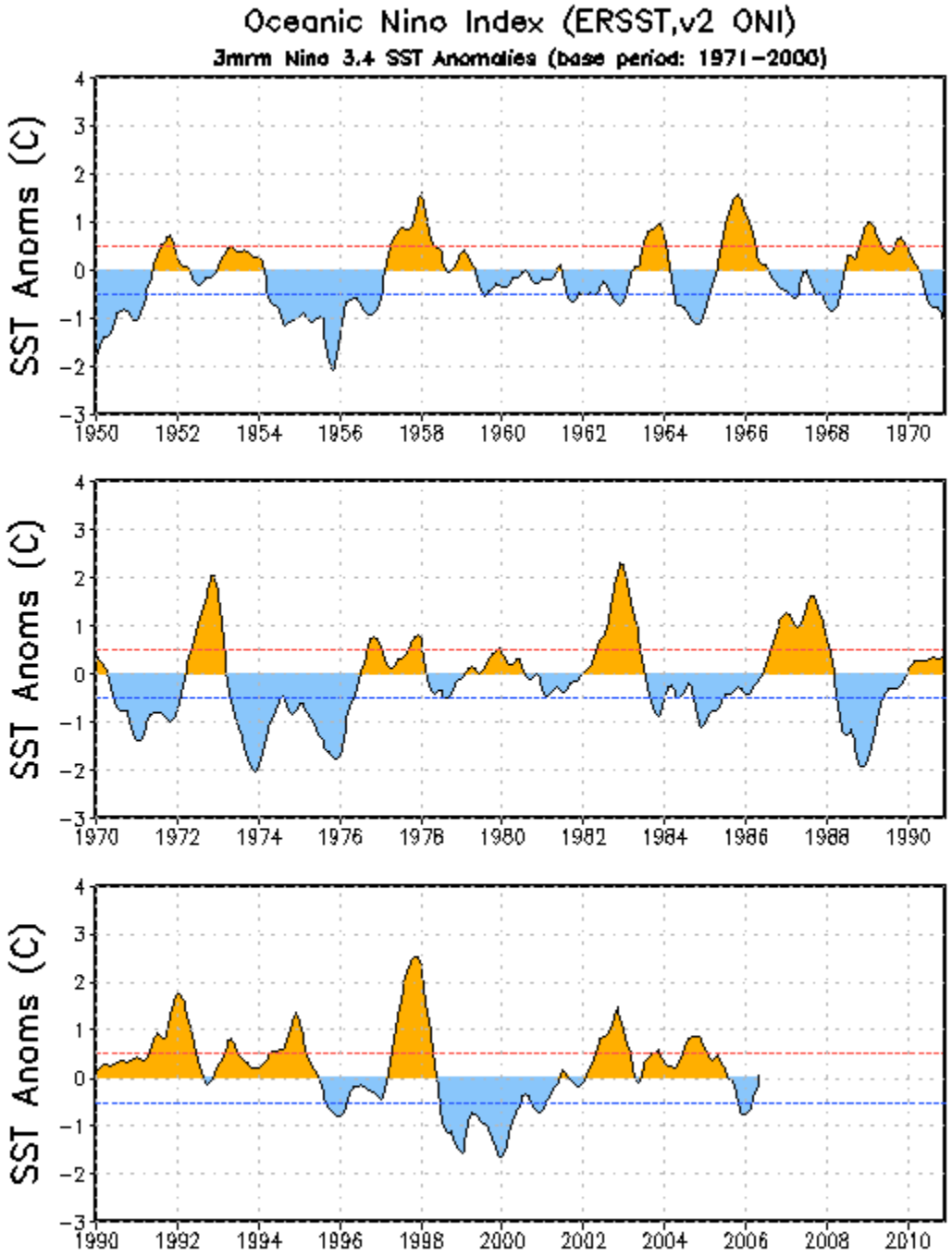

Figure 11. The Oceanic Niño Index (ONI) is the running 3-month mean SST anomaly for the equatorial Pacific and is the standard used by NOAA to identify El Niño (warm) and La Niña (cool) events in the tropical Pacific.

3. North Pacific

3.1 Atmospheric Circulation

In the winter of 2005/06, the atmospheric circulation was characterized by a high degree of variability. Specifically, December 2005 featured an anomalously strong Aleutian low, with sea-level pressure (SLP) in its center being 12 hPa below the long-term average. The North Pacific index (NPI), which is the area-weighted SLP over the region 30°N-65°N, 160°E-140°W (Trenberth and Hurrell, 1994), was 999.5, the record lowest value for December since 1899. It is particularly unusual that this abnormally low pressure occurred in the absence of an El Niño event, which is considered as one of the major factors leading to a stronger-than-normal Aleutian low (Lau 1996). Overall, the atmospheric circulation in December 2005 can be classified as W1, which is the most typical pattern associated with positive surface air temperature anomalies (SAT) in the eastern Bering Sea (Rodionov et al. 2005).

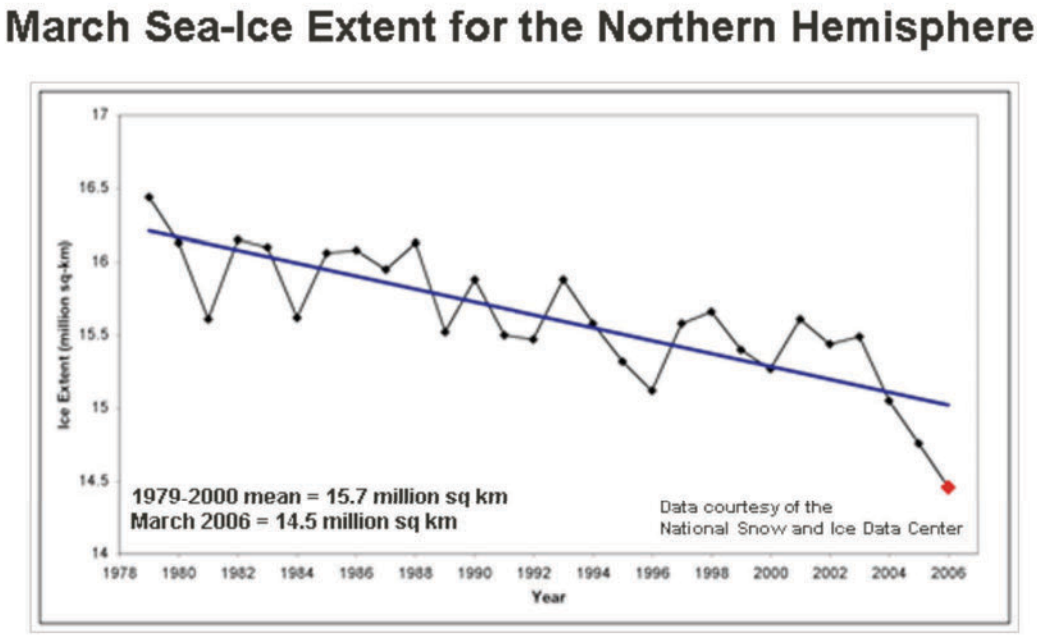

Figure 12. March sea-ice extent (in millions of square kilometers) across the Northern Hemisphere.

In January 2006, the Aleutian low was weak and split into two centers, one in the northwestern Pacific and the other one in the Gulf of Alaska. This pattern is classified as C1, which is the major circulation pattern for anomalously cold temperatures in the Bering Sea (Rodionov et al. 2005). Indeed, January SATs in the Bering Sea and Alaska were much below normal (see Temperature and Ice Cover in the Bering Sea, this report). The atmospheric circulation also featured anomalous middle to upper tropospheric troughing from the Gulf of Alaska into western Canada. This resulted in a near zonal flow over much of the Pacific-North American sector and advection of warm Pacific air masses deep into the continent, where monthly temperatures in much of the U.S. and Canada were above the 90th percentile of occurrences.

In February 2006, an anomalously high pressure cell in the central North Pacific strengthened even further, with SLP anomalies exceeding 12 hPa, and pushing the storm activity far north into the Bering Sea. The monthly NPI was the 6th largest for all Februaries since 1899. This extreme variability in atmospheric circulation over the North pacific is illustrated in Figure 13, which shows a time-latitude plot of SLP anomalies averaged for the meridional section 150°W-170°W. Although the high pressure cell weakened in the subsequent months, the NPI remained positive through June 2006.

3.2 Sea Surface Temperature Evolution

A sequence of by-monthly sea surface temperature (SST) anomaly maps from January-February 2006 to July-August 2006 is presented in Figure 14. These maps demonstrate two important features of SST evolution during the winter and spring of 2006: 1) the disappearance of negative SST anomalies in the central and eastern equatorial Pacific in association with the final stages of the weak La Niña episode, and 2) the development of a SST anomaly pattern in the North Pacific, with some elements of a negative Pacific Decadal Oscillation (PDO) phase. One of those elements is the strengthening and southward expansion of negative SST anomalies in the northeastern Pacific from January-February through, at least, May-June. This process was associated with the prevalent northwesterly anomalous wind over the eastern North Pacific in the first eight month of this year (Figure 15).

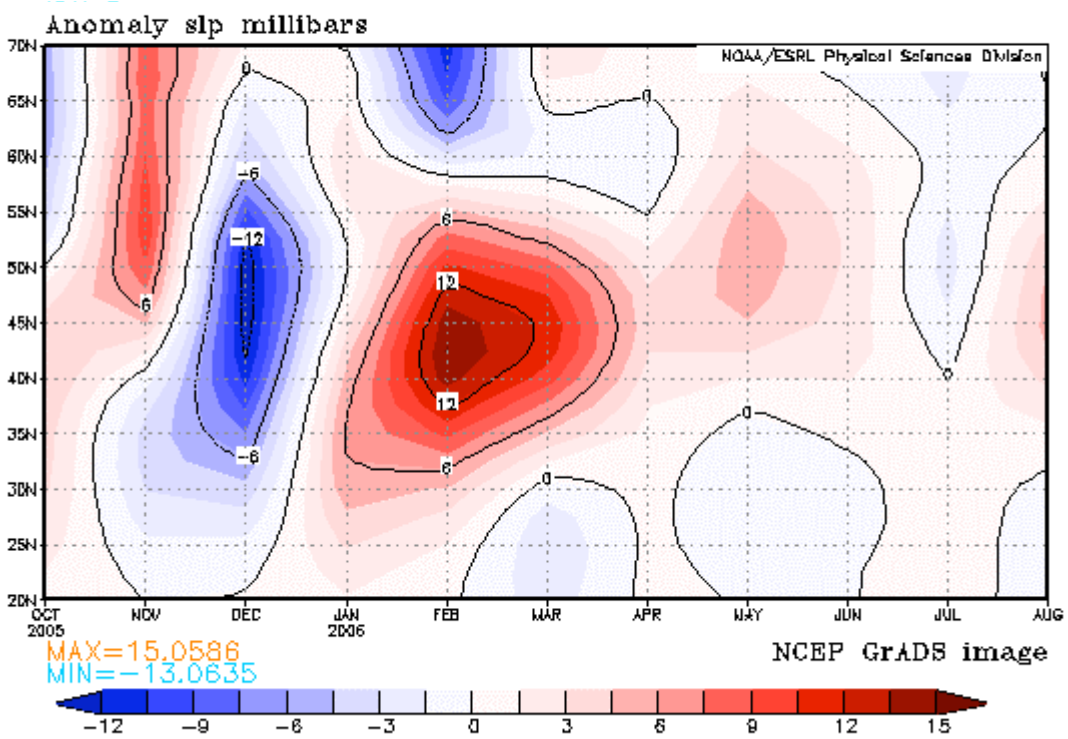

Figure 13. Time-latitude plot of SLP anomalies averaged over the meridional sector 150°W-170°W.

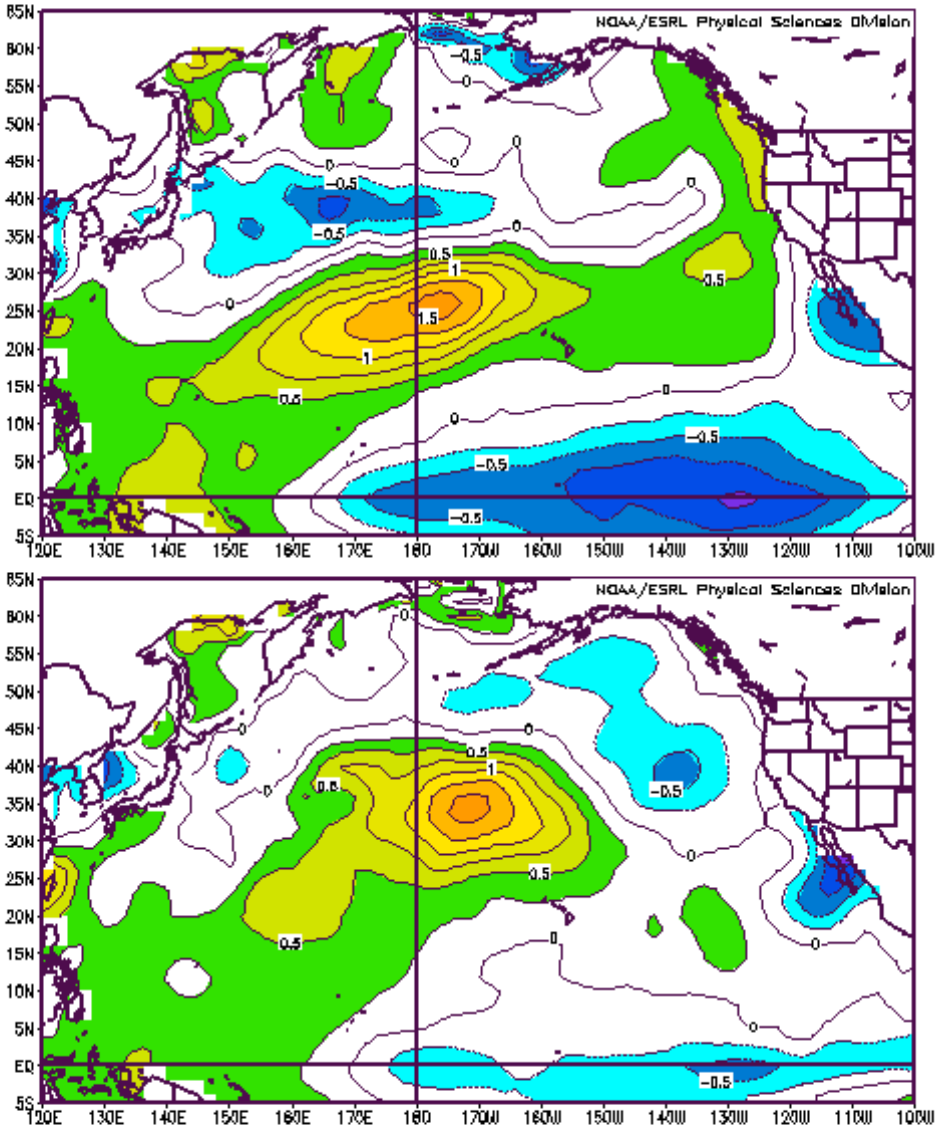

a) Jan-Feb 2006

b) Mar-Apr 2006

Figure 14. By-monthly SST anomalies (relative to 1971-2000 climatology) from January-February 2006 through March-April 2006.

c) May-Jun 2006

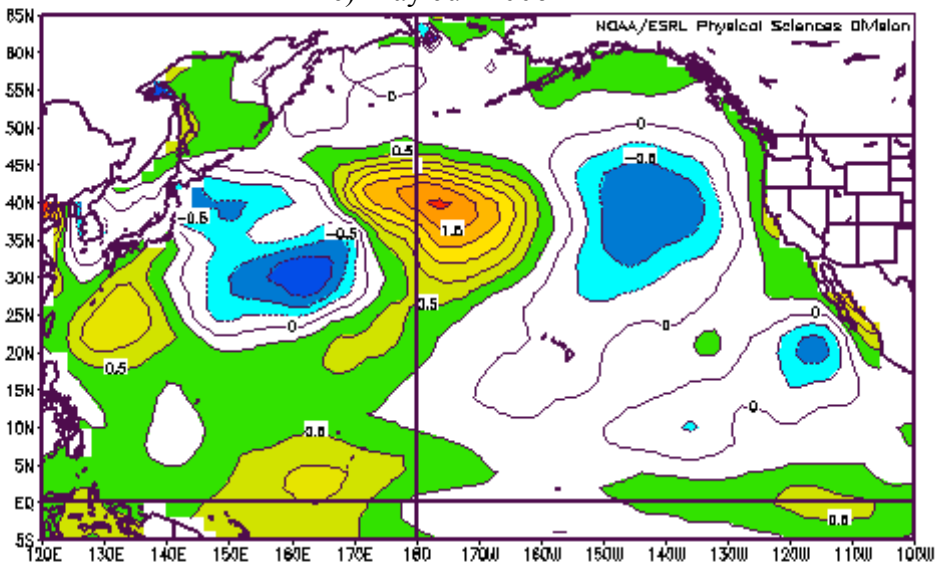

d) Jul-Aug 2006

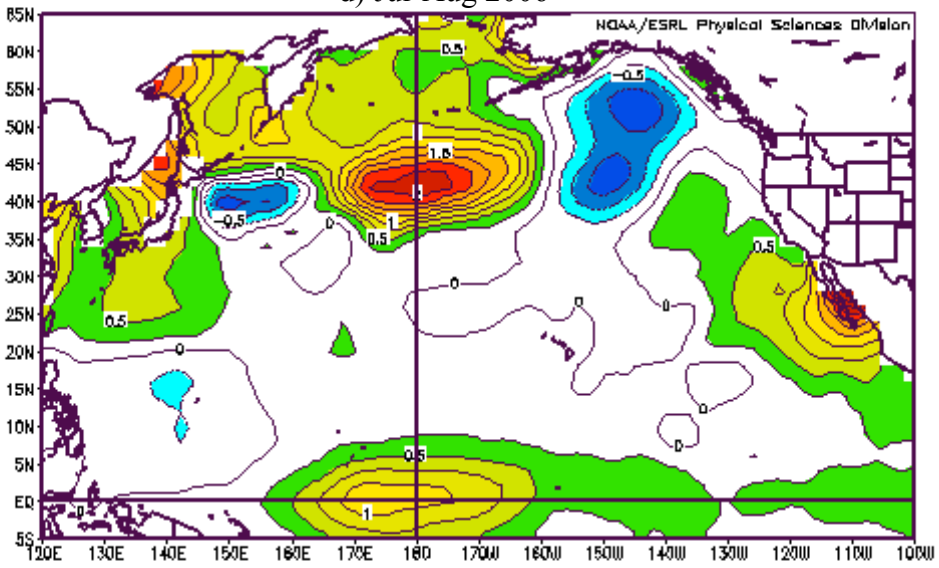

Figure 14 continued. By-monthly SST anomalies (relative to 1971-2000 climatology) from May-June 2006 through July-August 2006.

Another important aspect of the SST evolution in 2006 is the strengthening of the positive SST anomaly in the central North Pacific. The atmospheric circulation pattern, with its anomalous anticyclonic circulation over the basin (Figure 15), was conducive to this process. Several mechanisms contribute to the formation of a warm water pool under a high pressure cell over the central North Pacific. Anomalously high pressure implies less cyclonic activity in the area and hence less cloudiness, which means enhanced solar heating of the upper ocean. Strong easterly anomalous winds in the subtropical latitudes imply an enhanced transport of warm waters in the Ekman layer to the north and stronger than normal downwelling in center of the subtropical ocean gyre.

It is somewhat surprising, therefore, that in spite of atmospheric pressure and wind patterns that were characteristic of the negative PDO phase, that the monthly PDO index remained positive

through the first half of 2006. A contributing factor here is that the west Pacific was colder than normal, which projects on a positive phase of the PDO.

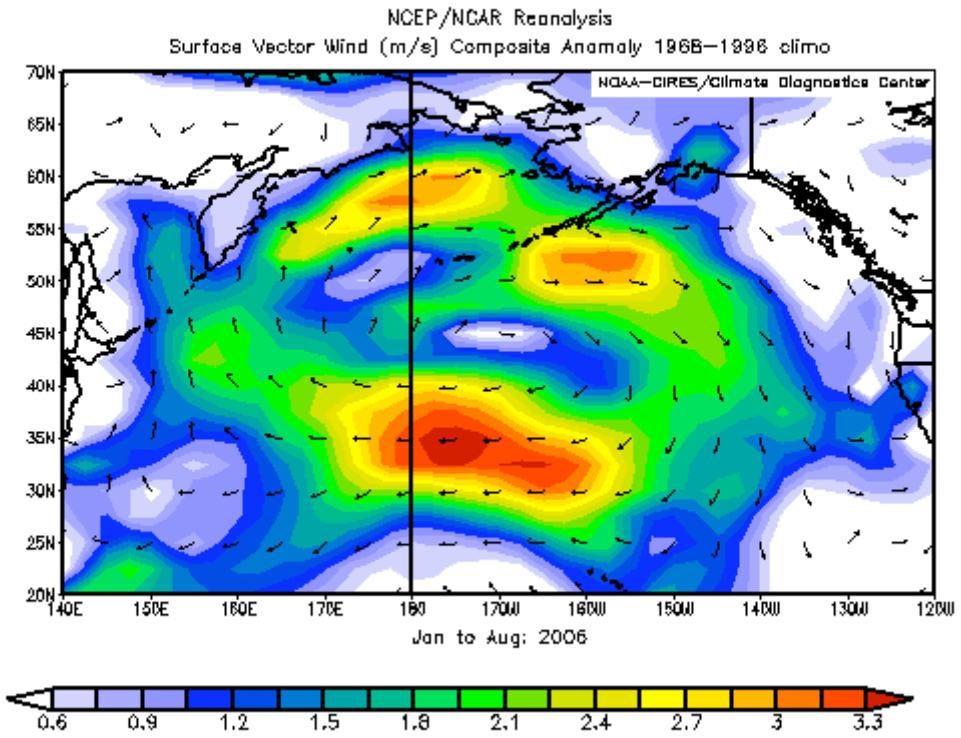

Figure 15. Surface vector wind anomalies averaged for the period from January 2006 through August 2006.

3.3 Sea Surface Temperature Forecast from NCEP

The latest seasonal forecast produced by the NCEP coupled forecast system model (CFS03) suggests that the atmospheric processes described above will continue to operate throughout the rest of the year and in winter and spring of 2007. The model suggest anomalously frequent troughing in the lower to middle troposphere along the North American west coast, which tends to promote negative SST anomalies in the Northeast Pacific. Anomalously cold waters east of Japan are forecast to warm up, and the entire pattern will resemble the negative phase of the PDO (Figure 16). Due to a probable El Niño event, a narrow strip of warmer than normal waters off the west coast of North America is likely to develop.

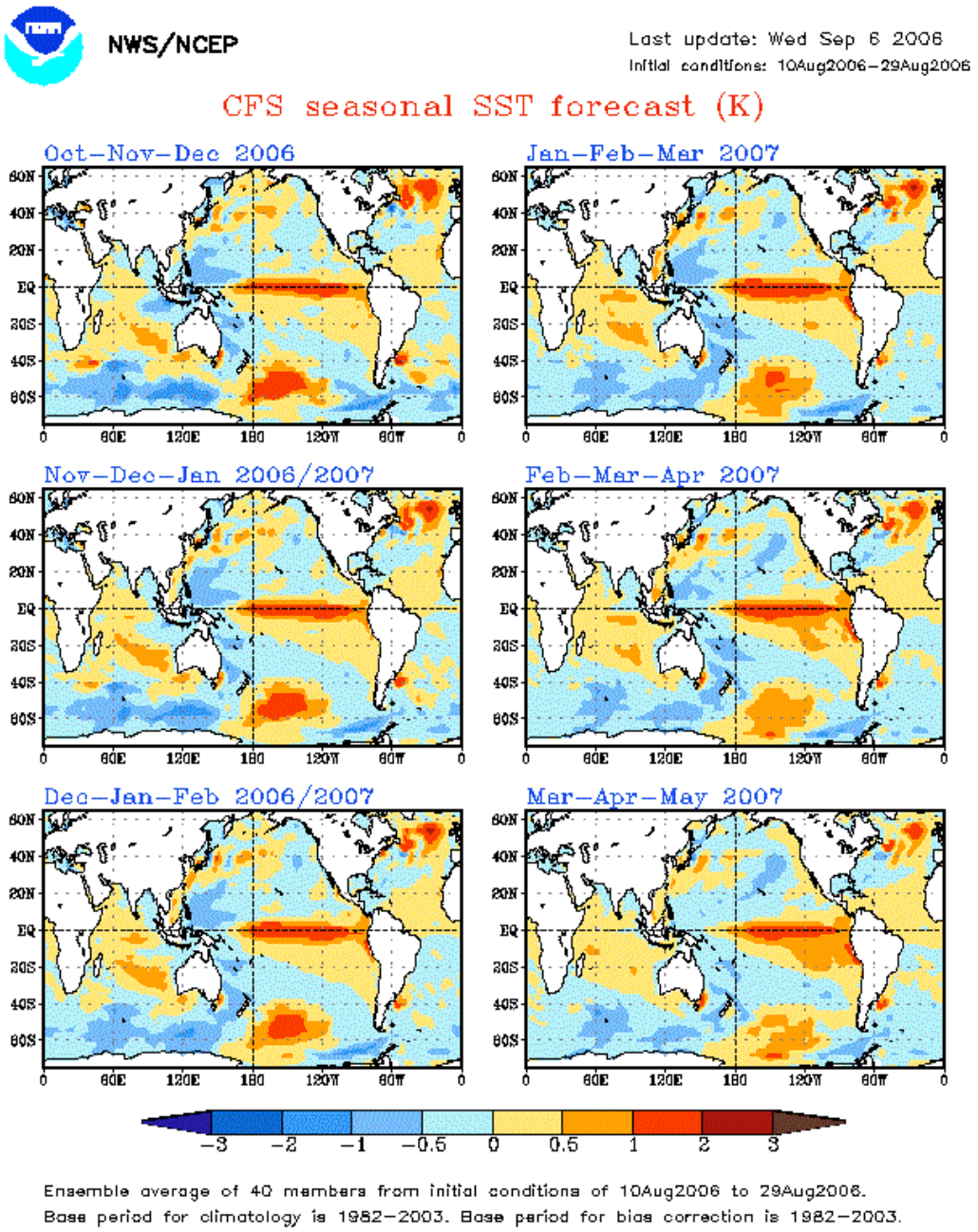

Figure 16. Seasonal forecast of SST anomalies from the NCEP coupled forecast system model.

4. Regime Shift Analysis

The NP index jumped to a positive value in the winter of 2005-06, which is characteristic of the weak Aleutian low regime of 1947-1976 (Figure 17a). Since this shift just occurred, it is uncertain whether it represents just a temporary change or actually heralds the beginning of a new regime. At the same time, the PDO index remained slightly positive (Figure 17b), which is more consistent with the current regime established since the late 1970s than for the previous regime of a PDO phase.

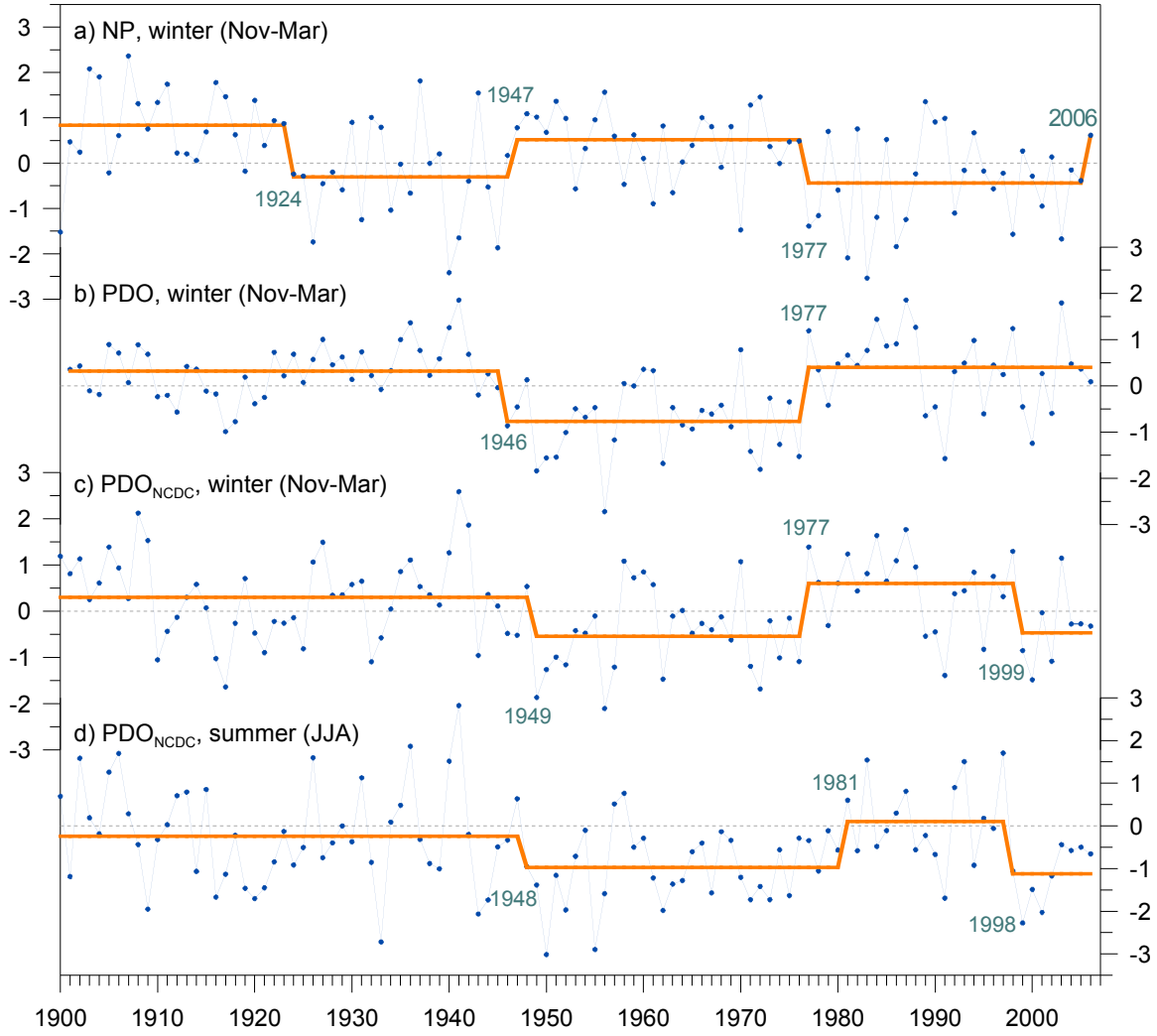

Figure 17. a) Winter (Nov-Mar) NP index from NCAR, b) Winter (DJF) PDO index from N. Mantua, University of Washington, c) Winter (DJF) PDO index from NCDC, and d) Summer (JJA) PDO index from NCDC. The stepwise trends (orange lines) were calculated using the sequential method (Rodionov 2004) with the cutoff length $l = 20$ years, probability level $p = 0.05$, and Huber weight parameter $h = 1$.

It should be noted that the data source used by N. Mantua (University of Washington) to calculate his index (Reynold's Optimally Interpolated SST) changed in 2002 from version 1 to version 2, and this could affect the values of the index. There is another PDO index calculated at the National Climate Data Center (NCDC) based on a single data source, the Extended Reconstructed SST data set. NCDC uses the same loading pattern as N. Mantua (University of Washington), but somewhat different technique to calculate the index. Although the correlation between the two variants of the PDO index is 0.87 (for the period 1901-2005), the implications for the regime shift analysis are substantial. Unlike the PDO index from N. Mantua (University of Washington), the PDO_{NCDC} index has a statistically significant (at the 0.01) level shift in 1999 (Figure 17 c). Since this year, there was only one positive value of the index in 2003 (a year of El Niño). The

magnitude of this shift is even greater for the summer PDO index (Figure 17d), being statistically significant at the 0.0007 level.

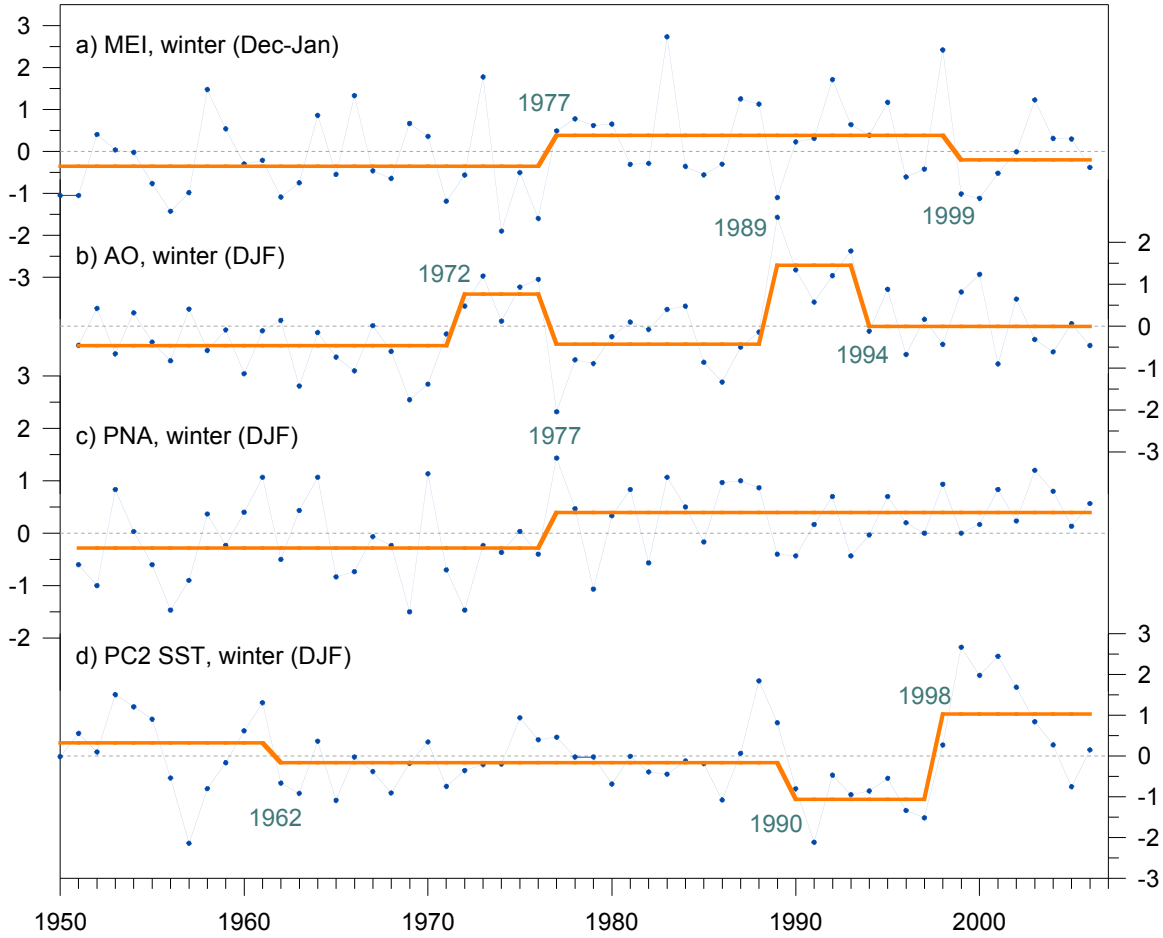

Figure 18. a) Winter (Dec-Jan) Multivariate ENSO index (l = 10, p = 0.3, h = 1), b) Winter (DJF) Arctic Oscillation index (l = 10, p = 0.2, h = 1), c) Winter (DJF) Pacific/North American index (l = 10, p = 0.1, h = 1), and d) Winter Victoria (PC2 SST) index (l = 10, p = 0.3, h = 1).

The indices presented in Figure 18 are available since the 1950s, and they were analyzed with a sequential method (Rodionov 2004) using less strict l (cutoff length in years) and p (probability level) parameters. The Multivariate ENSO index (MEI) shows an upward shift in 1977 and a downward shift in 1999 (Figure 18a). Despite relatively small magnitudes of the shifts (compared to those in the PDO), they are statistically significant at the 0.01 and 0.1 levels, respectively. The Arctic Oscillation (AO) index (Figure 18b), which jumped to its record high value in 1989, has substantially declined since then and can no longer serve as part of the explanation for the continuing Arctic warming (Overland and Wang, 2005). The Pacific/North American (PNA) teleconnection pattern is the leading mode of atmospheric circulation over the North Pacific and North America. The PNA index, obtained from the Climate Prediction Center (CPC), shows no sign of reversal from the high index regime established since 1977 (Figure 18c). The second empirical orthogonal function (EOF2) of SST in the North Pacific, also known as the Victoria pattern, accounted for much of the climate variability since 1990 (Bond et al. 2003). In the past several years, the principal component of this pattern (Figure 18d) declined to near zero values, and its role diminished. For more information on these and other climate indices, visit www.BeringClimate.noaa.gov.

GULF OF ALASKA

Pollock Survival Indices -FOCI

Contributed by S. A. Macklin, NOAA/PMEL
Contact: S.Allen.Macklin@noaa.gov
Last updated: August 2006

Using a conceptual model of early-life survival of western Gulf of Alaska walleye pollock (Megrey et al. 1996) for guidance, FOCI maintains several annual environmental indices. The indices are formulaic elements of a yearly prediction, during the year the fish are spawned, of the number of fish that will recruit as two-year olds. Some indices are determined qualitatively; the two reported here, seasonal rainfall at Kodiak and wind mixing in the exit region of Shelikof Strait, are determined numerically. Although data sources have changed somewhat over the years, chiefly with information used to estimate wind-mixing energy, every effort has been expended to make inter-year comparisons accurate and reliable.

Presently, the FOCI program is developing a modified approach (Megrey et al. 2005) to its annual forecast algorithm. When modifications are complete, it is probable that new indices will become available for this report. At the same time, it is possible that the indices presented here and in past years may be discontinued. Until a significantly long time series of new annual indices is available, the old indices will continue to be updated and published in this report.

Seasonal rainfall at Kodiak

Contributed by S. A. Macklin, NOAA/PMEL
Contact: S.Allen.Macklin@noaa.gov
Last updated: August 2006

FOCI uses measured Kodiak rainfall as a proxy for freshwater discharge that promotes formation of baroclinic instabilities (eddies) in the Alaska Coastal Current (ACC) flowing through Shelikof Strait (Megrey et al., 1996). Measured monthly rainfall amounts drive a simple model that produces an index of survival for age-0 walleye pollock. These young fish may benefit from spending their earliest developmental stages within eddies (Schumacher and Stabeno 1994). The model assumes that greater-than-average late winter (January, February, March) precipitation produces a greater snow pack. When the snow melts during spring and summer, it promotes discharge of fresh water through rivers and streams into the ACC. Similarly, greater than average spring and early summer rainfall, with their nearly immediate run-off, also favor increased baroclinity after spawning. Conversely, decreased rainfall is likely detrimental to pollock survival because they do not find the circulation features that promote their survival.

The time series of FOCI's pollock survival index based on measured precipitation is shown in Figure 19. Although there is large interannual variability, a trend toward increased survival potential is apparent from 1962 (the start of the time series) until the mid 1980s. Since then, the survival potential has been more level. Survival potential increased in 2003 and 2004 because almost all winter and spring months experienced average or greater rainfall than their respective 30-year averages. In 2005, precipitation remained somewhat above average but less so than in the previous two years. The 2006 season began with lower than normal precipitation during January, February and March. This decreased the potential for formation of baroclinic instabilities prior to and during spawning. April and May brought a return toward normal conditions, however the potential for instabilities forming from increased freshwater input to coastal water was still lower than expected. June was wet (at 151% of the 30-yr June average),

and this may have presented favorable habitat for late larval- and early juvenile-stage walleye pollock. Based on this information, the pollock survival potential for Kodiak 2006 rainfall is "weak to average". Interestingly, the precipitation-based survival index does not appear to track any of the long-term climate indices, e.g., AO, PDO, with any consistency, possibly because of the way winter and spring precipitation are used in the model. In the 3-yr running mean of the precipitation survival index, there is a change from decreasing to increasing survival potential in 1989. In that year, there was an abrupt shift in the AO.

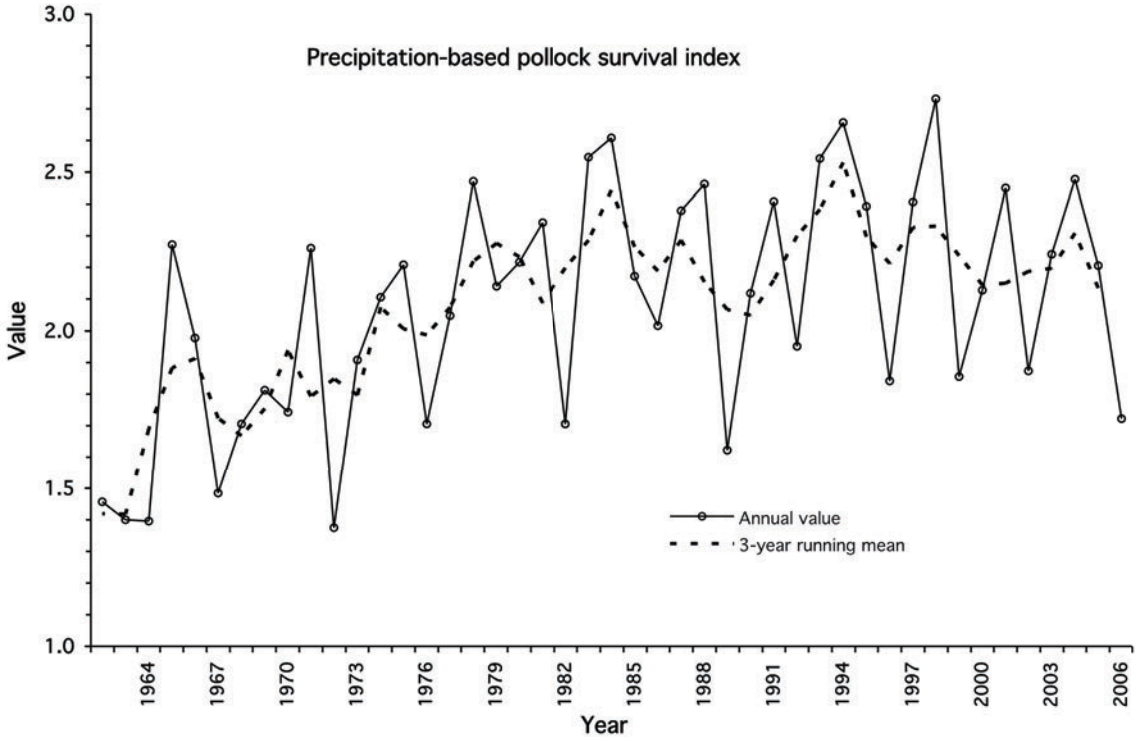

Figure 19. Index of pollock survival potential based on measured precipitation at Kodiak from 1962 through 2006. The solid line shows annual values of the index; the dashed line is the 3-year running mean.

Wind mixing at the southwestern end of Shelikof Strait
Contributed by S. A. Macklin, NOAA/PMEL
Contact: S.Allen.Macklin@noaa.gov
Last updated: August 2006

Rainfall is only one indicator of early-life-stage pollock survival. FOCI hypothesizes that a series of indices (proxies for environmental conditions, processes and relationships), assembled into a predictive model, provides a method for predicting recruitment of walleye pollock. A time series of wind mixing energy (W m^{-2}) at [57°N, 156°W] near the southern end of Shelikof Strait is the basis for a survival index wherein stronger than average mixing before spawning and weaker than average mixing after spawning favor survival of pollock (Megrey et al. 1996). The wind-mixing index is produced from twice-daily surface winds created from a model (Overland et al. 1980)

using NCEP reanalyzed sea-level-pressure fields. The model is tuned to the region using information determined by Macklin et al. (1993). A time series of the wind-mixing index is shown in Figure 20. As with precipitation at Kodiak, there is wide interannual variability with a less noticeable and shorter trend to increasing survival potential from 1962 to the late 1970s. Recent survival potential has been high relative to the early years of the record. Except for March 2003, March 2005 and June 2006, monthly averaged wind mixing in Shelikof Strait has been below the 30-year (1962-1991) mean for the last nine January through June periods (1998-2006). This may be further evidence that the North Pacific climate regime has shifted in the past decade.

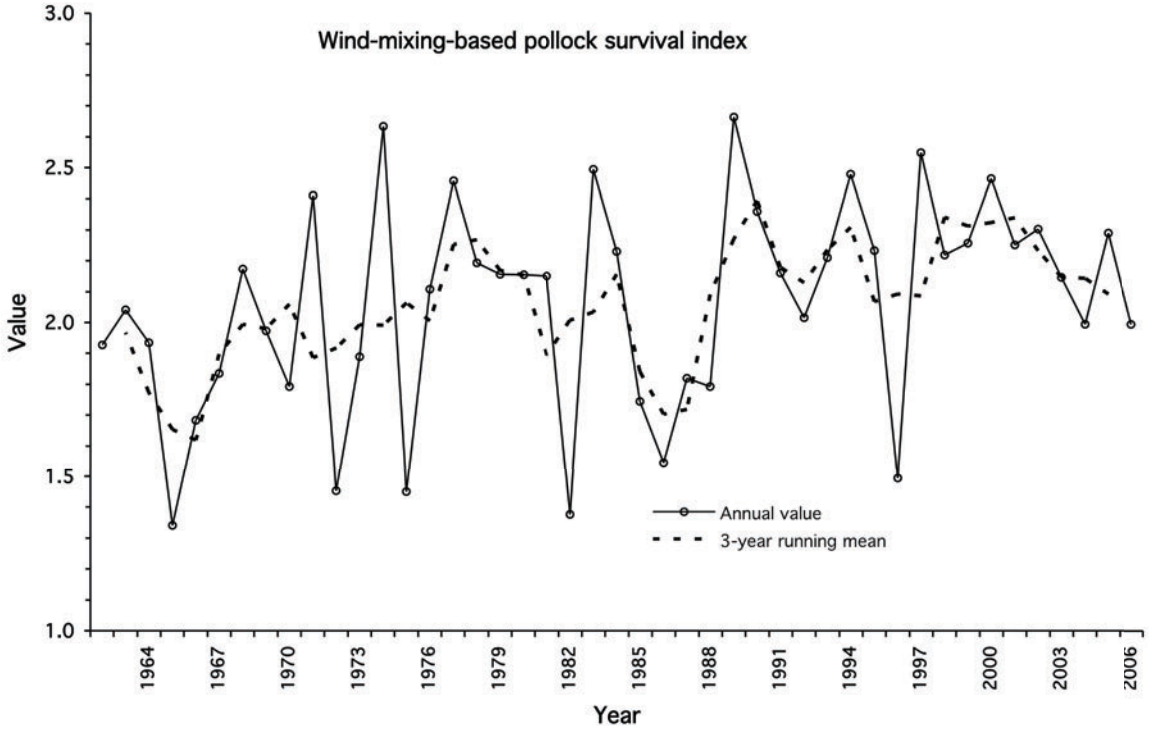

Figure 20. Index of pollock survival potential based on modeled wind mixing energy at [57°N, 156°W] near the southwestern end of Shelikof Strait from 1962 through 2006. The solid line shows annual values of the index; the dashed line is the 3-year running mean.

Ocean transport in the western Gulf of Alaska –FOCI
Contributed by P. J. Stabeno, NOAA/PMEL
Contact: Phyllis.Stabeno@noaa.gov
Last updated: November 2003

The spring and summer seasonal strength of the Alaskan Stream and Alaska Coastal Current (ACC) is an important factor for overall productivity on the shelf of the Gulf of Alaska. FOCI uses satellite-tracked drift buoys, drogued at mid mixed-layer depths (~45 m), to measure ocean currents as a function of time and space. Animations of drifter trajectories from deployments during 2001-2003 can be found at *http://www.pmel.noaa.gov/steller/ssl_drifters.shtml*. There is a strong seasonal signal in the ACC. During late spring and summer, the flow on the Gulf of

Alaska shelf between Prince William Sound and the Shumigan Islands is weak. The many bathymetric features such as troughs and banks interact with the currents. This results in flow up the eastern side of such troughs as Amatouli, Chiniak and Barnabas. Flow over banks such as Portlock, is often recirculating, and satellite-tracked drifters can be retained in closed circulation for weeks to months. ACC flow in the western Gulf of Alaska during 2001 and 2002 was particularly weak. Later in the summer or fall, with the intensification of regional winds, the ACC becomes stronger, and the flow down Shelikof Strait becomes more organized, as shown by the animations for September of 2001 and 2002. During 2003 (Figure 21), ACC flow was more organized and stronger. Specifically, the flow in Shelikof Strait appeared more complex with more meanders and eddies than have been evident in previous years. This year, more than the typical number of drifters went aground along the Alaska Peninsula and the Kenai Peninsula west of Gore Point.

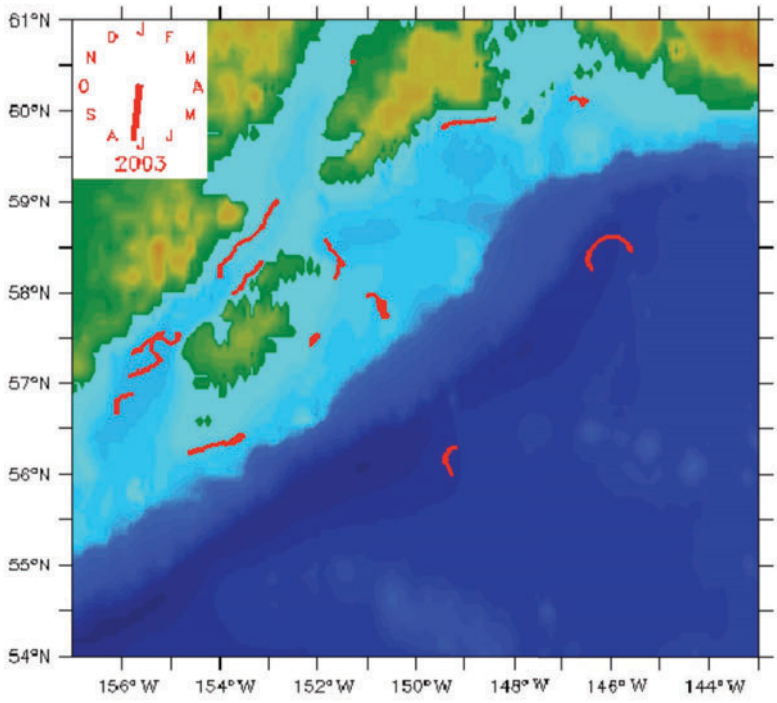

Figure 21. Tracks of satellite-tracked drifters for the period October 14-18, 2001, show sluggish flow on the shelf, except for within Shelikof Strait.

Cross-shelf fluxes are important to providing nutrients to the shelf. Each year (2001-2003) brought flow onto the shelf in the vicinity of the Seward Line, which extends south southeastward from the mouth of Resurrection Bay across the shelf and over the basin. The presence of an eddy is clearly evident from drift trajectories over the basin. Such eddies interact with the shelf, often drawing water off the shelf and into the basin, and are discussed in more detail in the next section. From the head of the gulf to Amchitka Pass, the Alaskan Stream appeared to be fairly typical during 2003, through July, with low eddy kinetic energy and relatively high velocity (>50 cm s^{-1} to the southwest). By next year, there will be enough data to allow construction of an annual Gulf of Alaska transport index that can be compared with climate indices such as PDO, AO, etc.

Eddies in the Gulf of Alaska – FOCI
Contributed by Carol Ladd, NOAA/PMEL
Contact: Carol.Ladd@noaa.gov
Last updated: September 2005

Eddies in the northern Gulf of Alaska have been shown to influence distributions of nutrients (Ladd et al. 2005) and phytoplankton biomass (Brickley and Thomas 2004) and the foraging patterns of fur seals (Ream et al. 2005). Eddies propagating along the slope in the northern and western Gulf of Alaska are generally formed in the eastern gulf in the autumn or early winter (Okkonen et al. 2001). In most years, these eddies impinge on the shelf east of Kodiak Island in the spring. Using altimetry data from 1993 to 2001, (Okkonen et al. 2003) found an eddy in that location in the spring of every year except 1998. They found that strong, persistent eddies occur more often after 1997 than in the period from 1993 to 1997.

Since 1992, the Topex/Poseidon/Jason/ERS satellite altimetry system has been monitoring sea surface height (SSH). Gridded altimetry data (merged TOPEX/Poseidon, ERS-1/2, Jason and Envisat; Ducet et al. 2000) allow the calculation of eddy kinetic energy (EKE). A map of eddy kinetic energy in the Gulf of Alaska averaged over the altimetry record shows three regions local maxima (labeled a, b, and c in Figure 22). The first two regions are associated with the formation of Haida eddies (a) and Sitka eddies (b). Regions of enhanced EKE emanating from the local maxima illustrate the propagation pathways of these eddies. Sitka eddies can propagate southwestward (directly into the basin) or northwestward (along the shelf break). The Sitka eddies that follow the northwestward path often feed into the third high EKE region (c; Figure 22). By averaging EKE over region c (see box in Figure 22), we obtain an index of energy associated with eddies in this region (Figure 23).

Figure 22. Sea surface height anomaly from TOPEX/Poseidon, ERS-1/2 and Jason merged altimetry. Positive anomalies imply anticyclonic circulation. Black box outlines region over which EKE was averaged for Figure 23.

The seasonal cycle (calculated from the entire time series) of EKE averaged over the box shown in Figure 22 exhibits high EKE in the spring (March – May) with lower EKE in the autumn (September – November). EKE has been high with a stronger seasonal cycle since 1999. Prior to 1999, EKE was generally lower than the ~13-year average, although 1993 and 1997 both showed periods of high EKE. Interestingly, the first 8 months of 2005 showed a return to the low EKE values observed prior to 1999. No significant eddies were observed in this region during the first half of 2005. This may have implications for the ecosystem. Phytoplankton biomass was probably more tightly confined to the shelf during this time period due to the absence of eddies. If fur seals have become dependent on eddies for foraging over the last five years of strong eddy variability, their foraging success may be negatively impacted this year. In addition, cross-shelf transport of heat, salinity and nutrients are likely to be smaller than in previous years with large persistent eddies. Research is ongoing as to the causes and implications of these patterns.

The altimeter products have been produced by the CLS Space Oceanography Division; downloaded from http://www.aviso.oceanobs.com/.

Figure 23. Eddy kinetic energy (EKE) averaged over the region shown in Figure 22 calculated from altimetry. Black: weekly EKE. Red: mean over entire time series. Green: annual cycle.

EASTERN BERING SEA

Temperature and Ice Cover – FOCI

S. Rodionov, P. Stabeno, J. Overland, N. Bond, and S. Salo, PMEL/NOAA
Contact: Sergei.Rodionov@noaa.gov
Last updated: November 2006

Summary. *Although the average seasonal characteristics of thermal conditions in the Bering Sea were close to normal, the winter of 2006 was characterized by a significant degree of month-to-month variability. In January surface air temperature (SAT) in St. Paul plunged to almost 2 standard deviations below normal. In the next two months SAT anomalies became positive, exceeding one standard deviation in March. These temperature swings were associated with a restructuring of atmospheric circulation patterns over the North Pacific. Spring months were colder than normal, and ice extent was south of its normal position. The ice retreat index indicates that ice stayed in the vicinity of Mooring 2 for almost 1.5 months after March 15, which is much longer than in the previous six years. Sea surface temperatures in May were the coldest since 1999, which suggests a more extensive cold pool than normal in the summer of 2006. A cold spring and late ice retreat were, probably, the most important features of the physical environmental conditions in 2006.*

In an overall sense, the winter of 2006 in the Bering Sea was close to normal, but contrasts to the warm conditions of the recent decade. The mean winter (DJFM) surface air temperature (SAT) at St. Paul was -3.18˚C, or 0.44˚C above the average for the base period 1961-2000 (Figure 28a). The Bering Sea pressure index (BSPI) remained negative, as it had been since 1998. Negative (positive) values of the BSPI indicate predominance of cyclonic (anticyclonic) conditions in the region. The ice cover index (a combination of several highly correlated ice-related variables) was slightly positive (Figure 29a) and the ice retreat index (IRI) indicates that ice stayed for 46 days after March 15 in a 2° x 2° box (56-58°N, 163-165°W) around Mooring 2 in the southeast Bering Sea (Figure 29b).

These average numbers, however, do not reflect the substantial month-to-month variability that occurred in the Bering Sea. As shown in Figure 30, after a relatively mild December, SAT at St. Paul dropped in January to -8˚C, which was 4.7˚C below the 1961-2000 average. It was the coldest January since January 2000. In February 2006, SAT rebounded to 1.6˚C above the average, and in March it was 3.5˚C above the average. Later in the spring, however, SAT anomalies were on the cold side again. These month-to-month variations in SAT are associated with a restructuring of atmospheric circulation over the North Pacific from a strong Aleutian low in December to a weak and split Aleutian low in January. A high pressure anomaly that formed over the central North Pacific in January strengthened even further in February and March. During these last two months, however, storms were frequent in the high latitudes bringing warm Pacific air into the Bering Sea (For details on atmospheric circulation see the Pacific Climate Overview section).

The high degree of variability within the 2006 winter season is also seen in ice cover, presented in Figure 31 as a percentage of ice in the 2˚ x 2˚ box (56-58°N, 163-165°W) surrounding Mooring 2. Ice appeared in the box in mid-January, which is an average start date of the ice season there (Figure 32). Due to very cold weather in January, ice quickly extended south, covering more than 80% of the box. Anomalously mild and stormy weather occurred in February and March causing ice to retreat as quickly as it arrived. Because of cold weather spells later in spring, ice peaked again around April 1 and May 1. Ice finally cleared the box in the second week of May, which made the IRI the highest since 1999 (Figure 29b).

It is interesting that the Bering Sea was about the only place in the Arctic where sea ice extent anomalies in January 2006 were positive and ice extent was south of its median position for the period 1979-2000 (Figure 33, top panel). By March 2006, however, sea ice concentration anomalies were negative practically everywhere along the periphery of Arctic ice extent (Figure 33, middle panel). The total Arctic sea ice extent for this month was 14.5 million sq. km., or 1.2 million sq. km. below the 1979-2000 mean value. This makes March 2006 the record low March for the entire period of observations since 1979. In April sea ice in the Bering Sea advanced again. Figure 34 illustrates how far south the ice edge was compared to the previous five years. In May, sea ice concentration anomalies in the Bering Sea remained positive, and sea ice extent was much father south than its median position for this month (Figure 33, bottom panel).

Due to anomalous ice cover extent, average sea surface temperature (SST) over the eastern Bering Sea in May was sharply lower (Figure 35). May SST is a good predictor of summer bottom temperatures and the extent of the cold pool. Although sea ice concentration in the eastern Bering Sea between 57°N and 58°N (Figure 36) was not particularly high after early February, especially as compared with other heavy ice years, ice stayed longer in the area than in any other year since 1999. Mooring 2 records indicate 2006 has been a remarkably cold year, mainly because the ice persisted into May and heating of the water column did not really begin until late May (Figure 37). In contrast, 2005 was the warmest year on record at the Mooring 2 site, since 1995 (Figure 37). Bottom temperature data for the summer of 2006 was unavailable at the time of writing, but given the relatively late ice retreat, it is strongly suspected that the cold pool was the most prominent it has been since 1999. The extent of the cold pool relates not only to the near-bottom habitat, but also impacts the overall thermal stratification and ultimately the mixing of nutrient-rich water from depth into the euphotic zone. Regarding the latter process, June-July wind mixing at M2 during 2006 (not shown) was the strongest since 1996, and the second strongest since 1979. We do not know yet whether the upper mixed layer was anomalously thick in 2006 like it was in 1996. All in all, it appears that the most important aspect of the physical environmental conditions in the eastern Bering Sea during 2006 was the unusually late retreat of the sea ice in the spring.

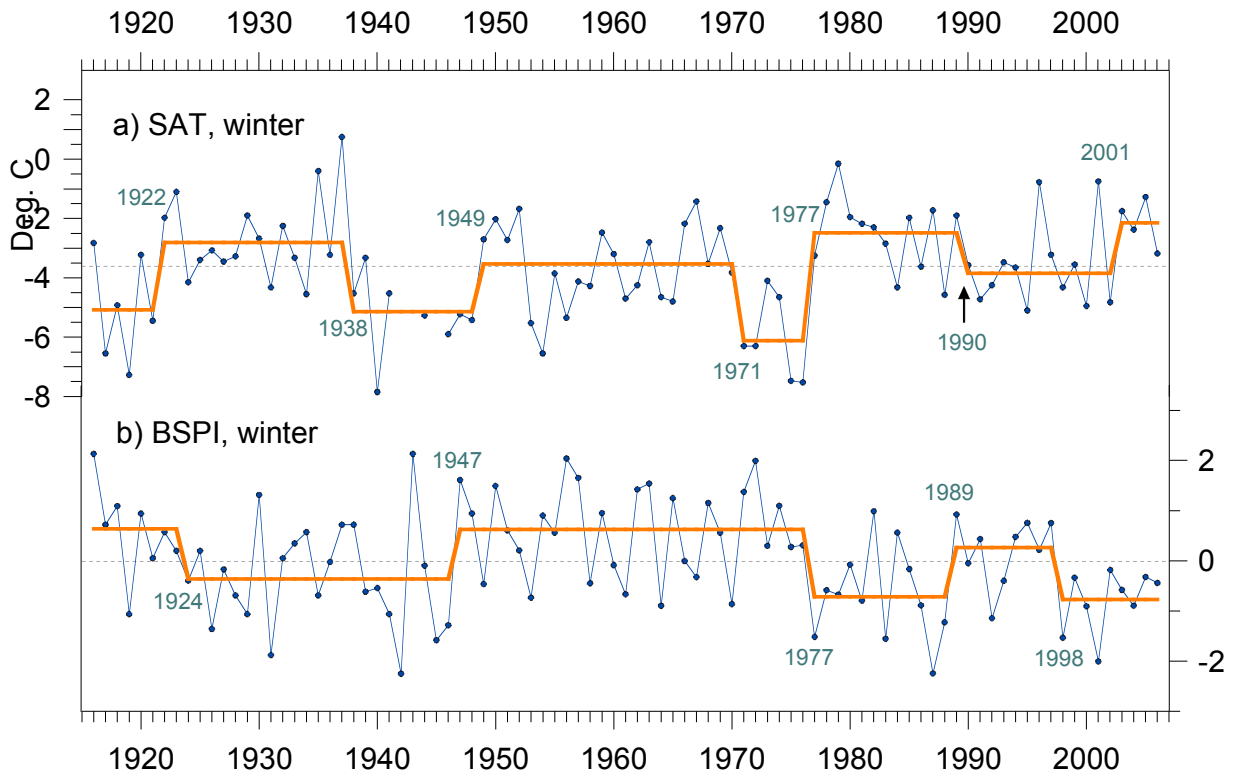

Figure 28. Mean winter (DJFM) a) surface air temperatures in St. Paul, Pribilof Islands and b) Bering Sea pressure index. The dashed line for the top graph indicates the mean SAT value of -3.62˚C for the base period, 1961-2000. The stepwise functions (orange lines) characterize regime shifts in the level of fluctuations of the variables. Shift points were calculated using the sequential method (Rodionov 2004), with the cutoff length of 10 years, significance level of 0.2, and Huber weight parameter of 1.

.

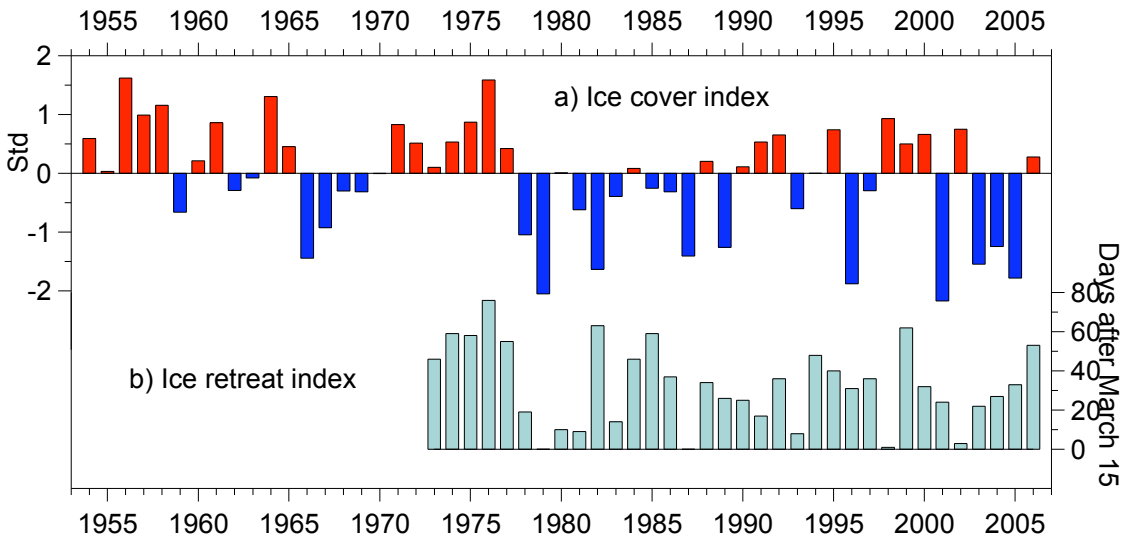

Figure 29. a) Ice cover index, 1954-2006, and b) ice retreat index, 1973-2006.

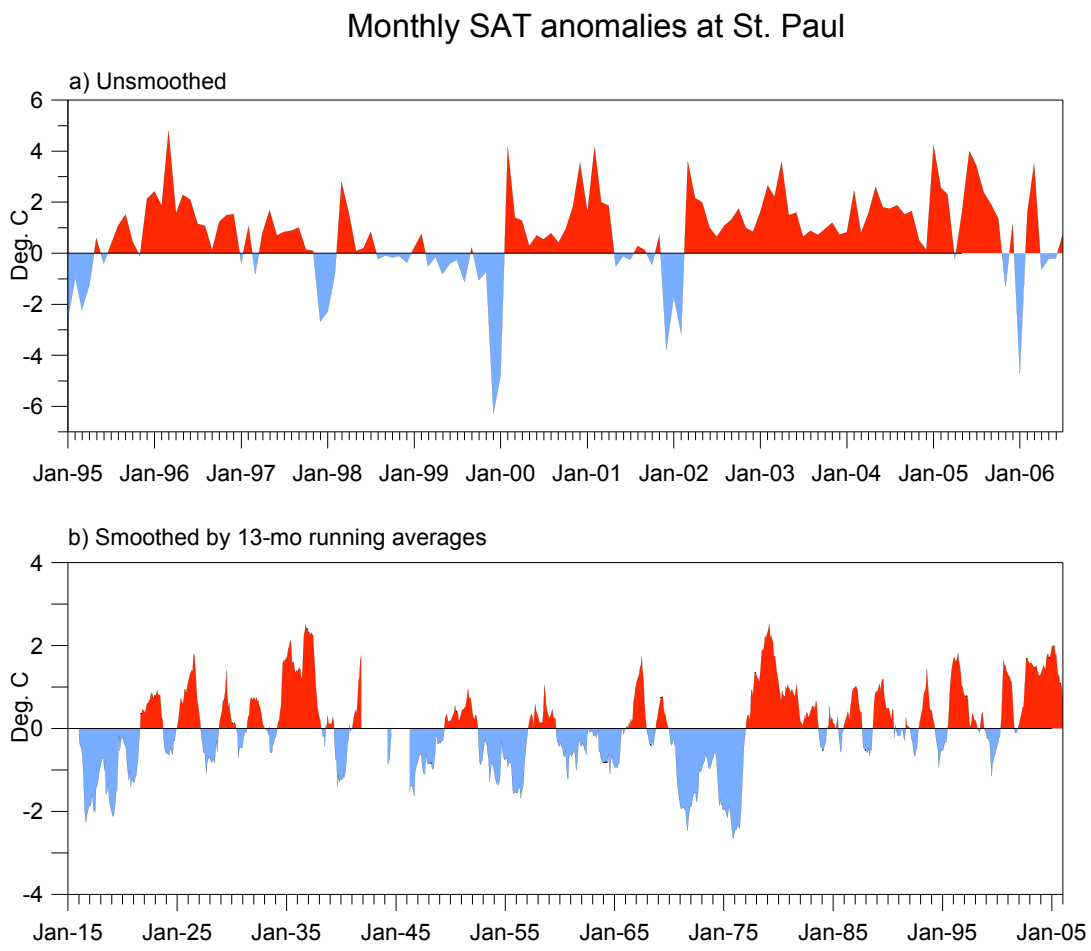

Figure 30. Mean monthly surface air temperatures anomalies in St. Paul, Pribilof Islands, a) unsmoothed, January 1995 through July 2006, and b) smoothed by 13-mo running averages and referred to the central month of the window, January 1916 through January 2006. The base period for calculating anomalies is 1961-2000.

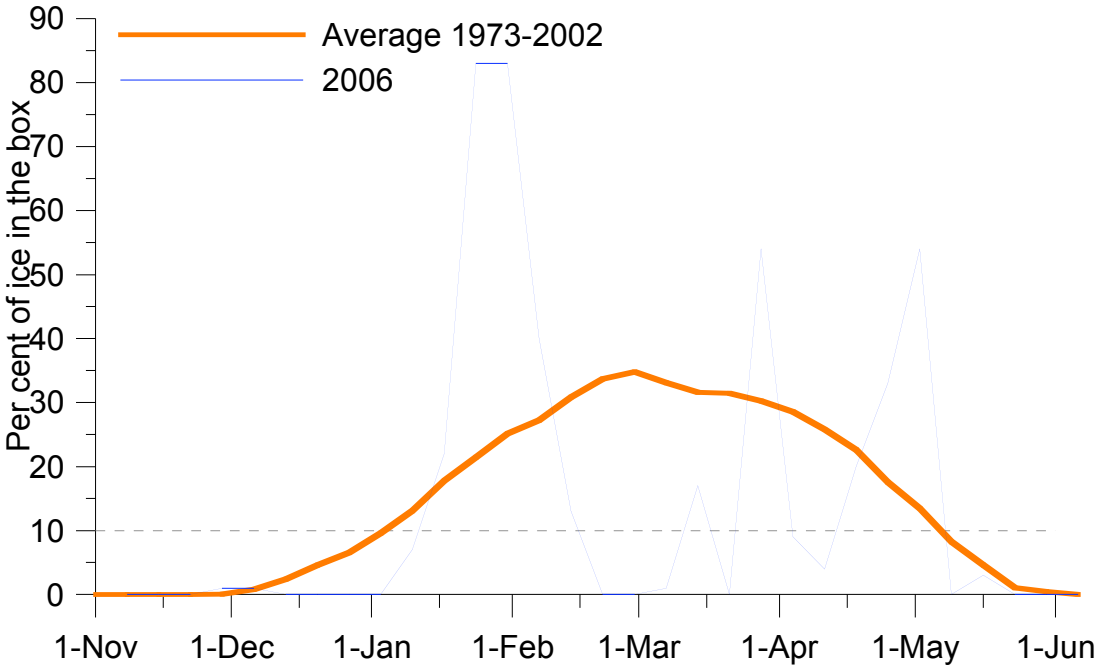

Figure 31. Percentage of ice in the 2˚ x 2˚ box (56-58°N, 163-165°W) during the winter of 2006.

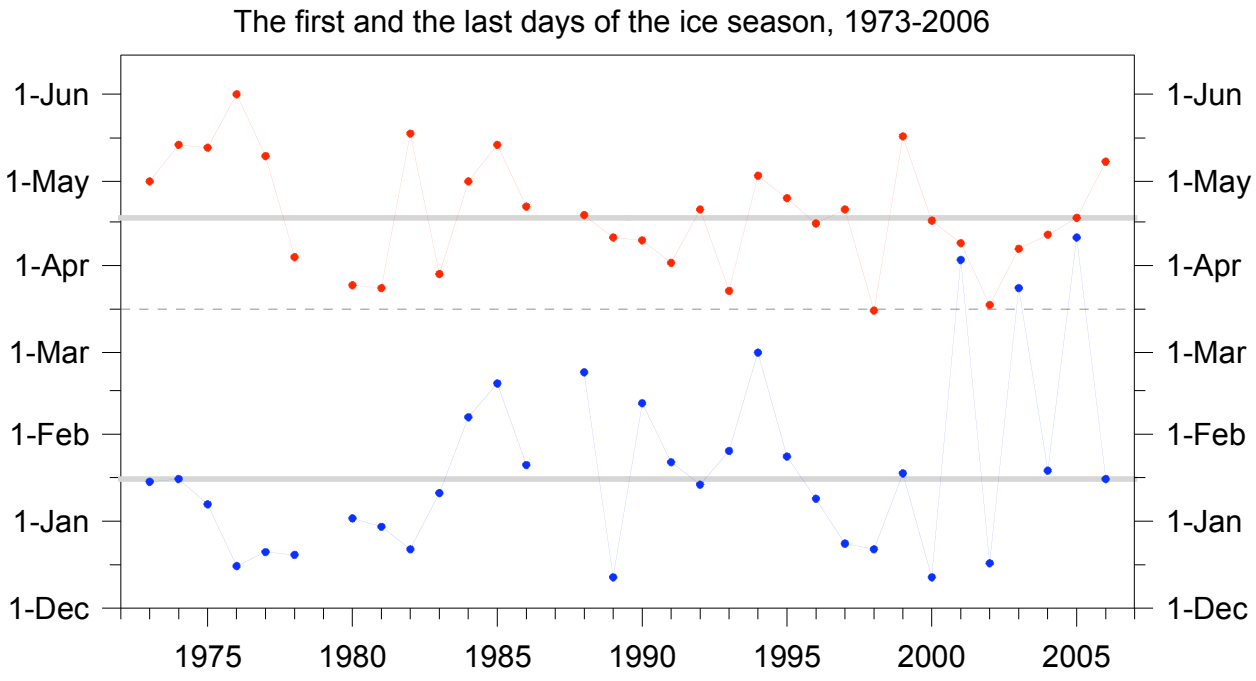

Figure 32. The first and last days of the ice season, 1973-2006. The gray solid horizontal lines are the mean dates for these two variables. The dashed line (March 15) is used as a threshold to calculate the ice retreat index. No ice was present in the box in 1979 and 1987.

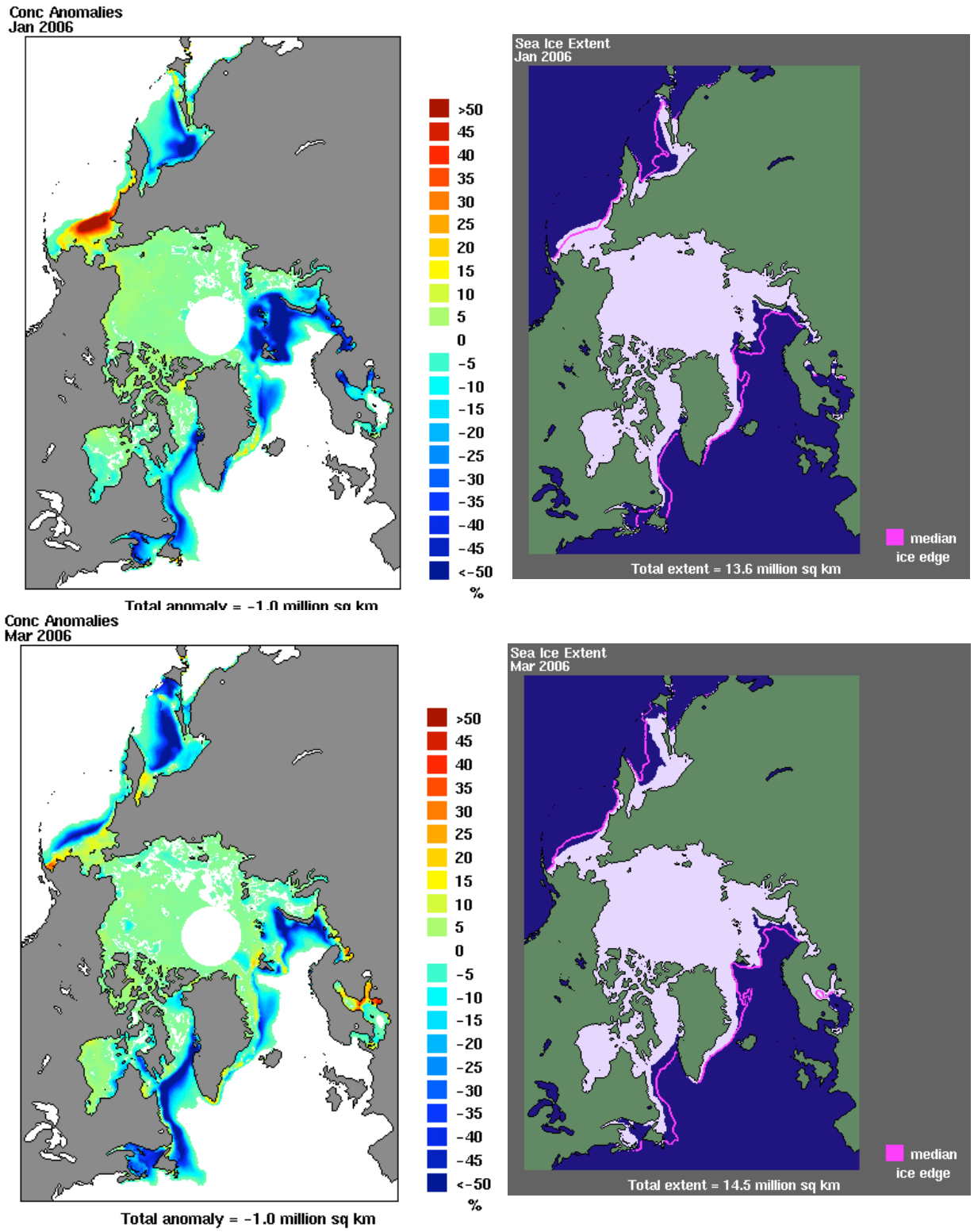

Figure 33. Sea ice concentration anomalies (left column) and extent (right column) in the Arctic during January (top panel), March (bottom panel) and May (next page) 2006.

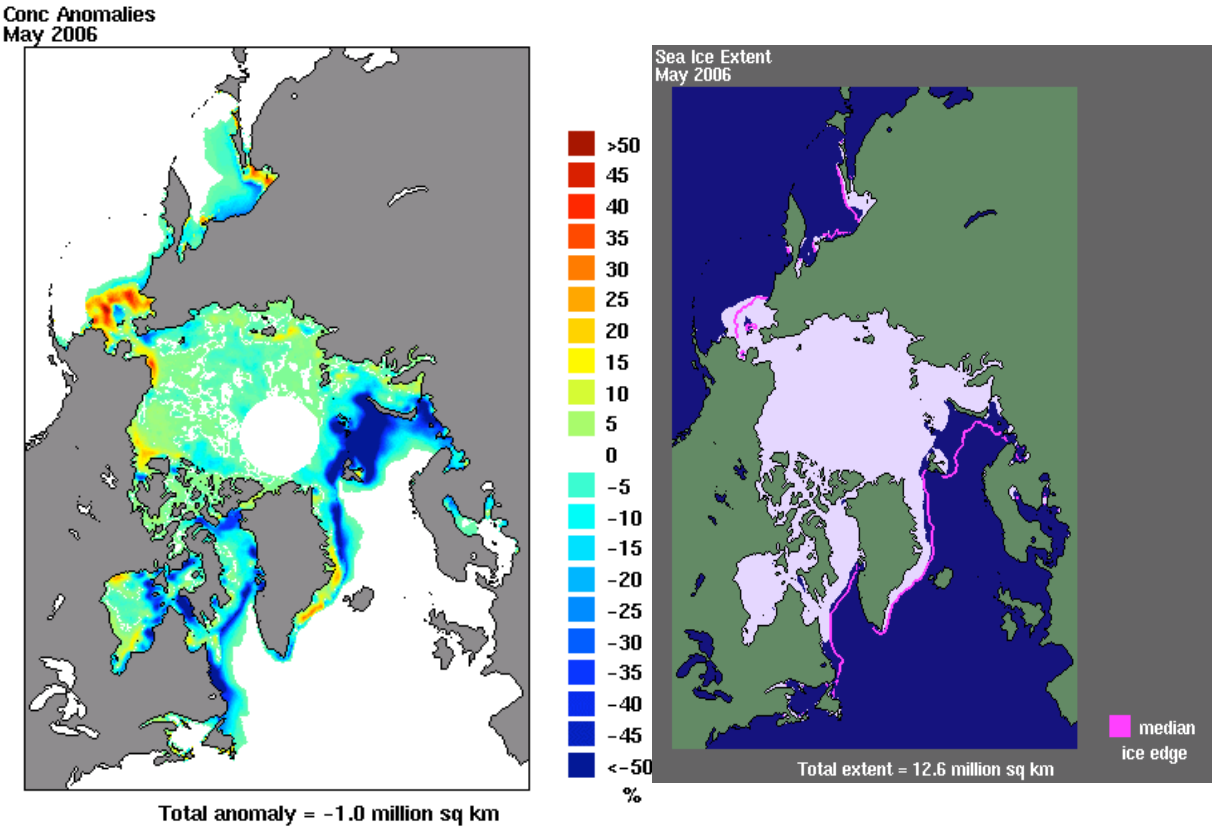

Figure 33. (continued). Sea ice concentration anomalies (left column) and extent (right column) in the Arctic during May 2006.The base period for anomalies is 1979-2000.

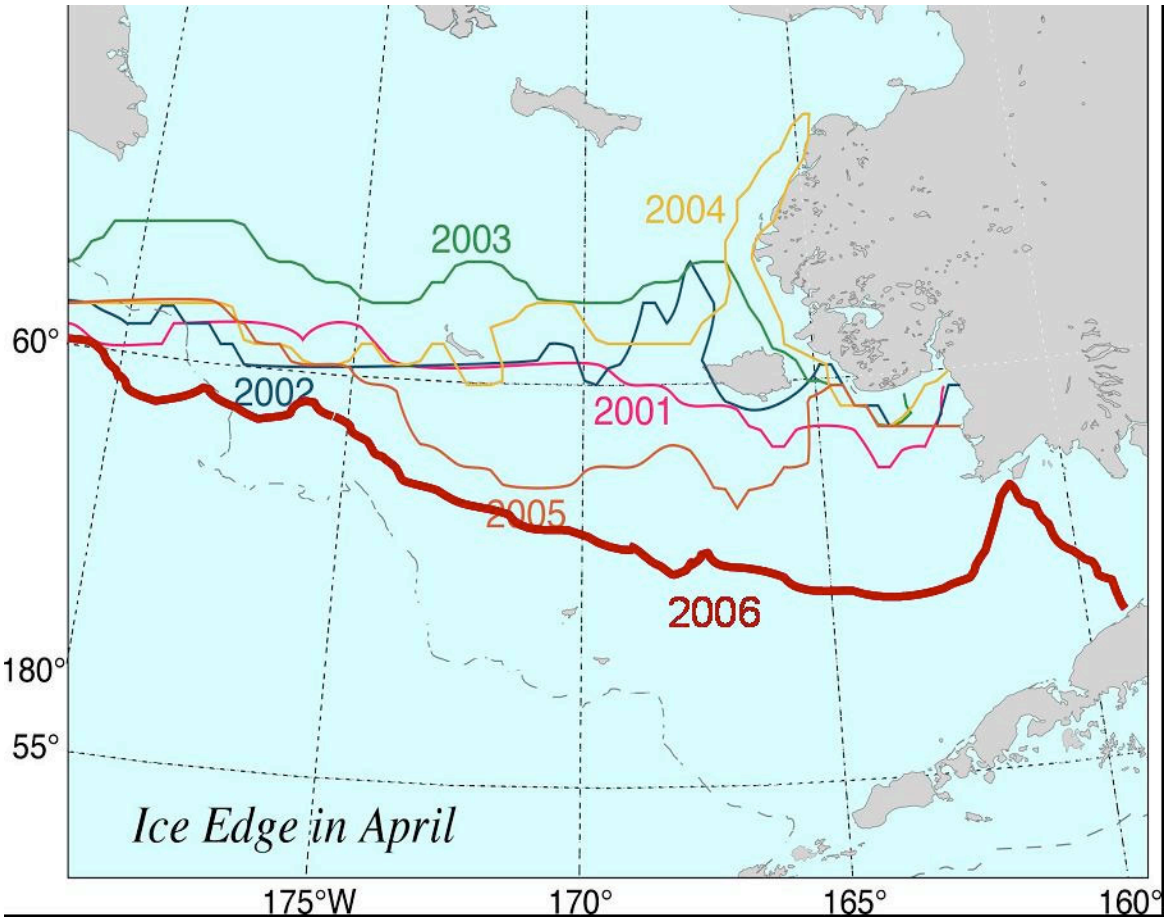

Figure 34. Ice edge in April 2006 in comparison to the previous five years.

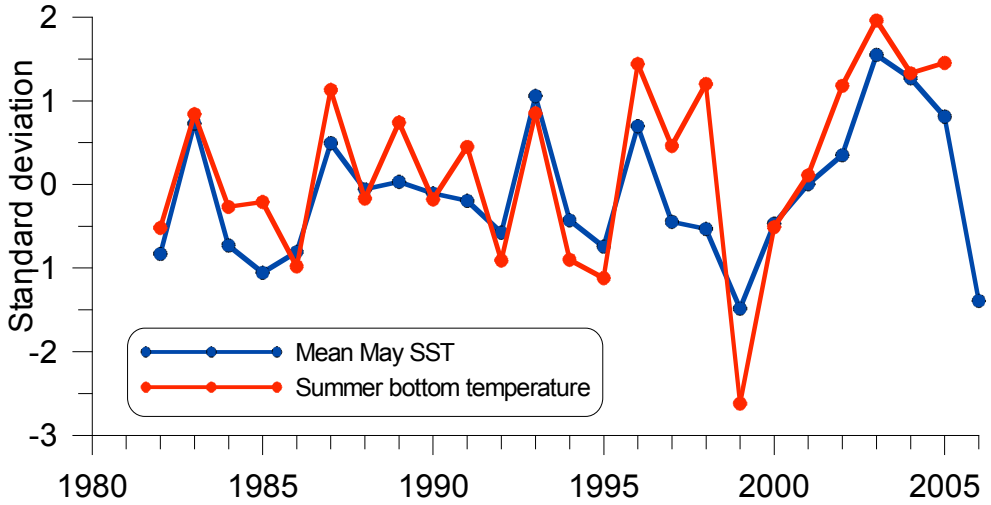

Figure 35. The MaySST index and mean summer bottom temperature in the southeastern Bering Sea, 1982-2006.

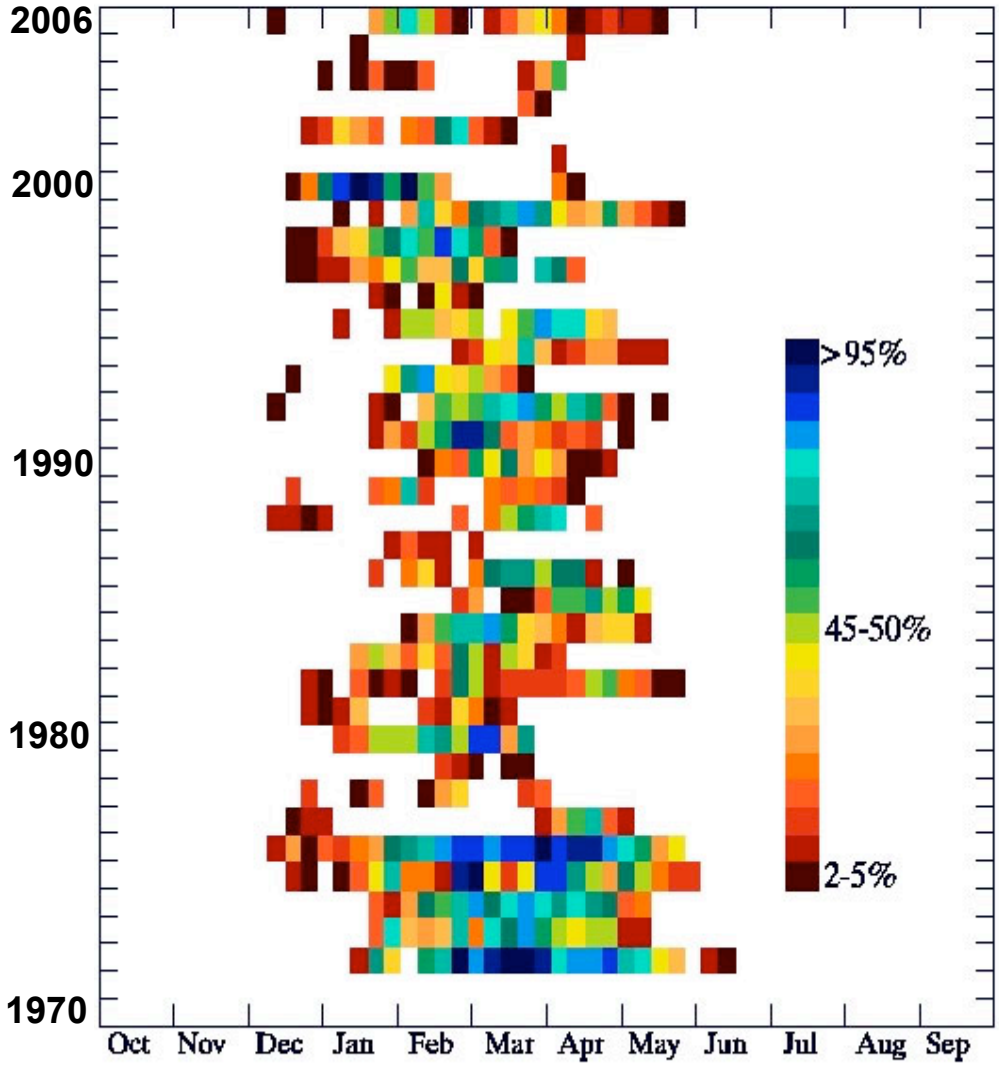

Figure 36. Percent of ice coverage between 58°N and 60°N in the eastern Bering Sea, 1972-2006.

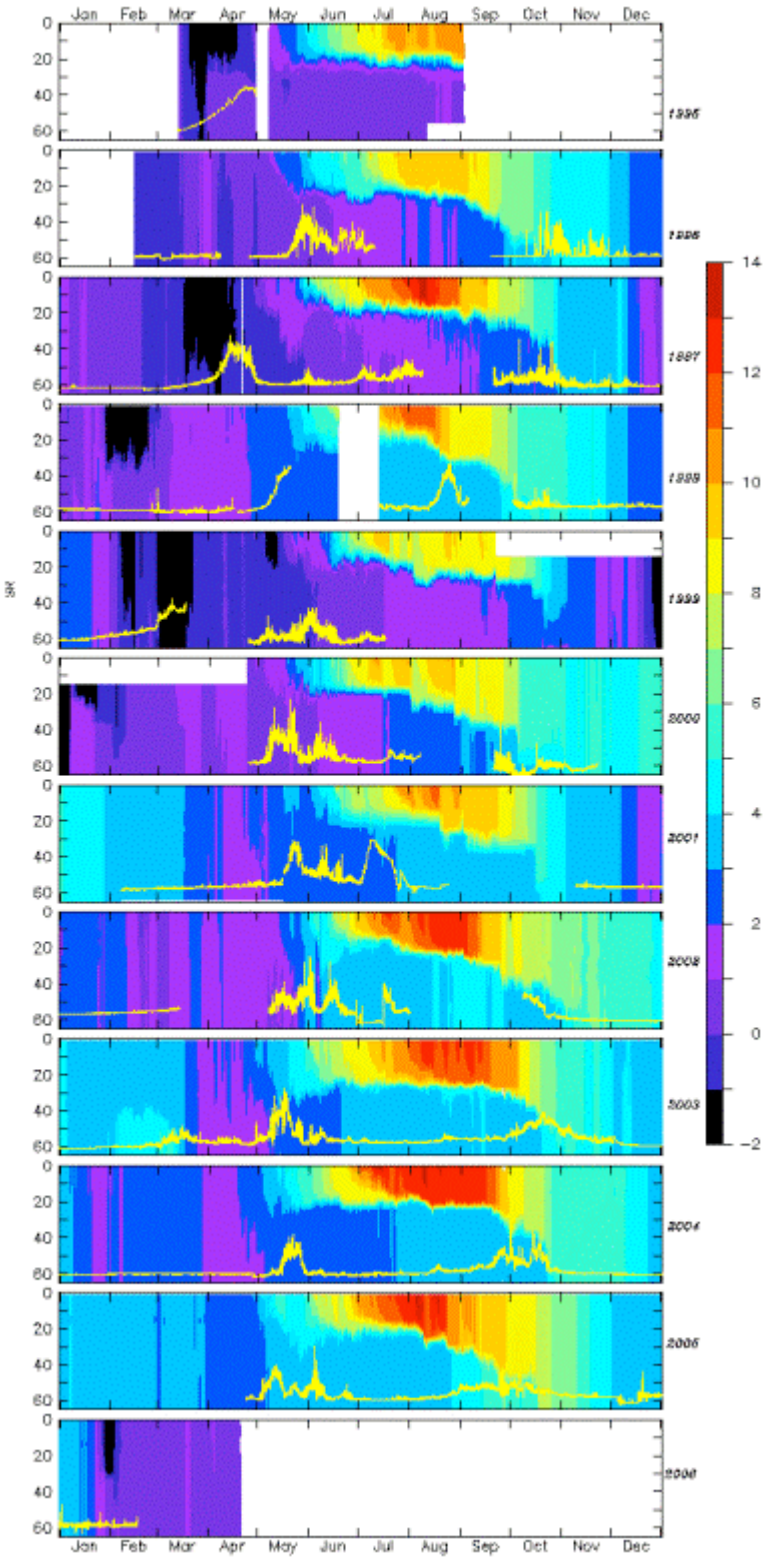

Figure 37. Contours of temperature measured at Mooring 2, 1995-2006. The coldest temperature (black) occurred when ice was over the mooring. The yellow line is fluorescence measured at ~11 m. Note that early blooms are associated with the presence of ice.

Simulated Drift Trajectories in the Southeast Bering Sea –FOCI

Contributed by Dylan Righi, FOCI, NOAA/PMEL
Contact: Dylan.Righi@noaa.gov

Last updated: November 2004

One of the most important resources in the Bering Sea (both for economic value and for its role in the ocean ecosystem) is the walleye pollock (*Theragra chalcogramma*) fishery. In the 1998, 50% of the world ocean catch of pollock came from the Bering Sea (Napp et al. 2000). At the same time walleye pollock (especially juveniles) are the main prey of other fishes, seabirds and marine mammals, meaning changes in stock size exert pressure on the entire Bering Sea food web. There are large inter-annual variations in pollock recruitment (Wespestad 1993) that must be understood in order to successfully manage this fishery. Climate variability and physical forcing play an important role in recruitment of fish and shellfish species (Wespestad et al. 2000; Wilderbuer et al. 2002; Zheng and Kruse 2000). Pollock recruitment is understood to be mainly set by their first year (Kendall and Duker 1998) and one fate that young pollock meet is cannibalism by adult pollock. Thus, transport of pollock eggs and larvae to regions of high adult density should adversely affect survival. Wespestad et al. (2000) test this hypothesis by using a surface transport model (OSCURS, (Ingraham and Miyahara 1988)) to simulate egg/larvae trajectories, and hindcasting survival rates. We attempt to improve on this work by using a full primitive equation ocean model to calculate trajectories instead.

We have used the northeastern Pacific Regional Ocean Model System (ROMS) to simulate trajectories in the southeastern Bering Sea. Drifter tracking in ROMS is done using a fourth order predictor-corrector scheme and allows vertical movement. We currently have results for the years 1996-2003. The simulated drifters are initialized in the Bering Sea just north of Unimak Island and to the northeast of Unimak Pass. This is known to be an area of spawning for walleye pollock (Hinckley 1987). The initial drifter positions fill out a seven by seven grid with horizontal separations of about 10 km (Figure 38). Vertically, there are 15 drifters initialized at each grid point with maximum depths just over 40 m. The drifter initial positions are denser near the surface, replicating vertical egg distribution data collected in the Bering Sea (Kendall et al. 1994). Drifters are released on April 1 of each year and are tracked for 90 days.

Endpoints after 90 days for drifter trajectories from the 1998-2003 runs are shown in Figure 39 (this plot shows all drifters at all depths). In all years there is a strong tendency for trajectories to move to the northeast up the Alaskan peninsula. The other common path is movement to the northwest along the 100-m isobath. The split between these two paths is seen clearly in the 1998, 1999, 2001 and 2003 drifter endpoints. The full trajectory plots (not shown here) show that the endpoints in 2000 are the result of a strong turning to the northwest of trajectories that had been moving up the Alaskan peninsula. In 2002 the drifters initialized at deeper points follow the common paths along the peninsula and the 100-m isobath. But drifters nearer the surface seem influenced by local winds and first move to the northeast, then turn to the northwest, resulting in endpoints spread evenly across the entire shelf. Further study of possible forcing mechanisms is needed to understand what leads to these years departing from the archetypal two-limbed flow.

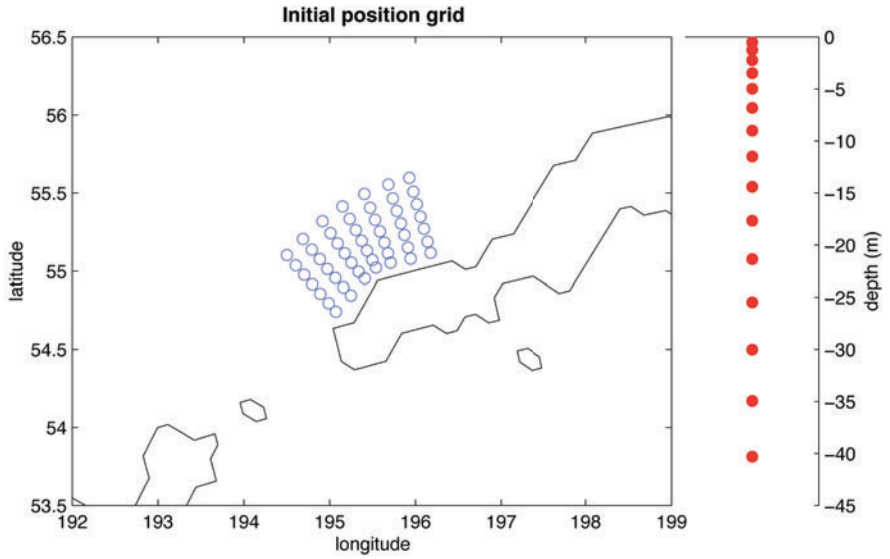

Figure 38. Simulated drifter initial horizontal (left) and vertical (right) positions.

The initial goal of this work was to compare simulated trajectories from a full primitive equation model with those from the Ocean Surface Current Simulations (OSCURS) numerical model. OSCURS computes daily surface current fields using daily sea level pressure and long-term mean geostrophic current data. As such, it is a simpler model in terms of the physics involved but is much more computationally inexpensive. Wespestad et. al. (2000) used OSCURS to create simulated trajectories in the Bering Sea. The initial grid used here was centered on the initial release point they used. Our trajectories for drifters released near the surface (0 to 5 m depth) show good agreement with the OSCURS results. But our results show variation of trajectory endpoints with changes in both horizontal and vertical initial position. Figure 40 shows the full trajectories for the 2001 simulated drifters. The upper left panel shows the tracks of all the drifters released, while the upper right and the bottom panels show drifter tracks as a function of their release depth. Within each depth bin it is evident that there is a large dependence of drifter endpoints on initial vertical placement with each bin showing, to relative degrees, the two-limbed split flow.

There is also a strong dependence on release depth. The OSCURS 2001 trajectory (not presented here) moves a short distance to the northeast up the Alaskan peninsula as do the majority of the NEPROMS drifters released in the upper 5 m of the water column (upper right panel of Figure 40). But with deeper release points comes a stronger divergence of the trajectory fates. In the 5-20 m and 20-40 m release bins there are significant numbers of drifters that join the 100-m isobath flow to the northwest, with some even moving through Unimak Pass before turning back. OSCURS results would completely miss this variation in particle fates.

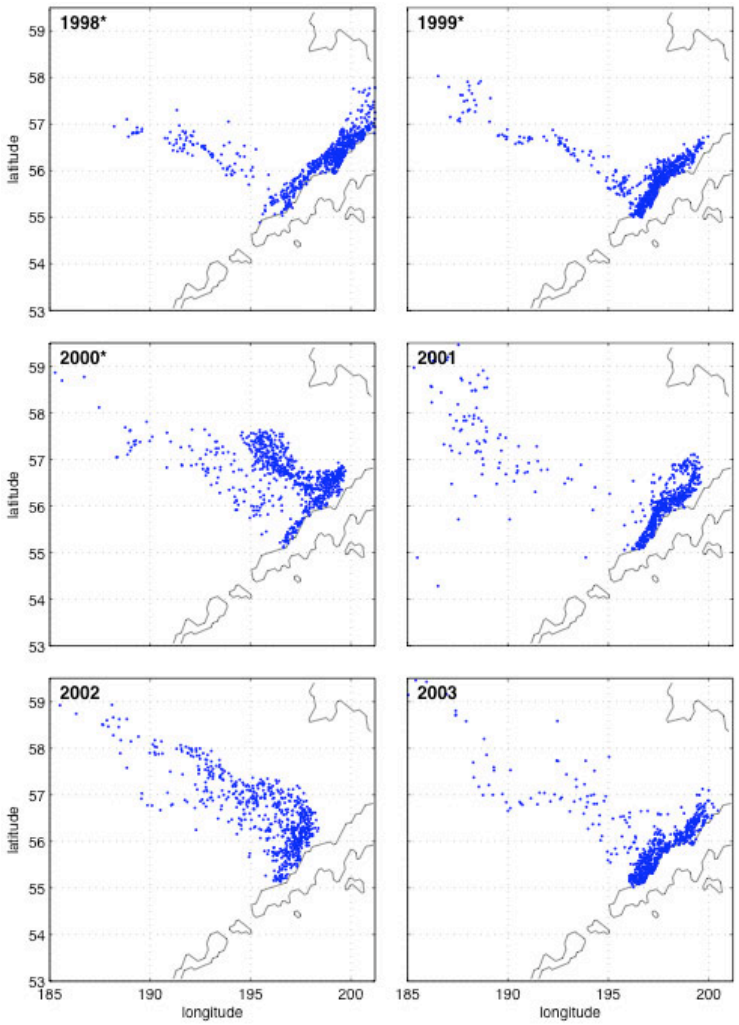

Figure 39. Endpoints for 90-day drifter trajectories for 1998-2003.

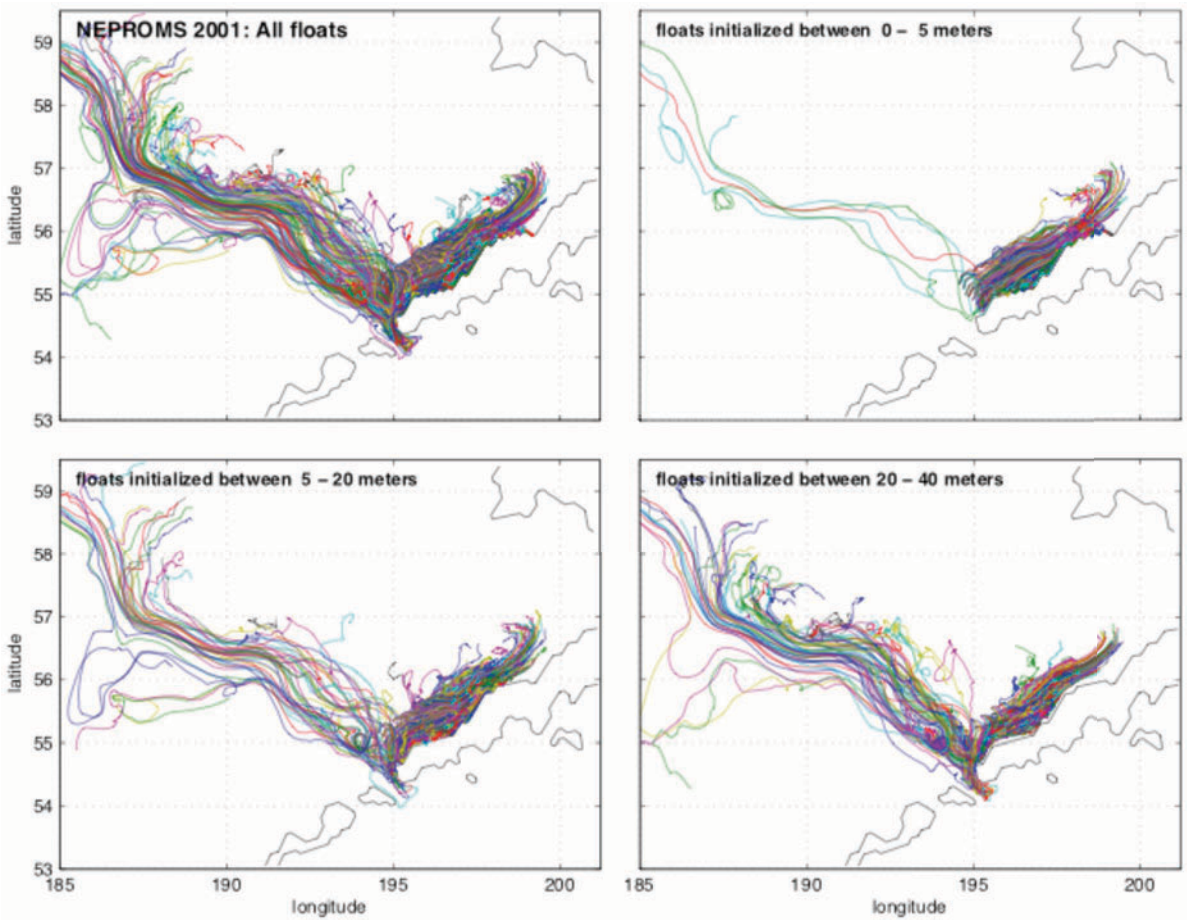

Figure 40. Full trajectories for the 2001 90-day simulated drifters. Upper left panel shows all drifters, while the upper left and bottom panels show drifters divided as a function of initial release depth.